Colloidal silica rods in electric fields
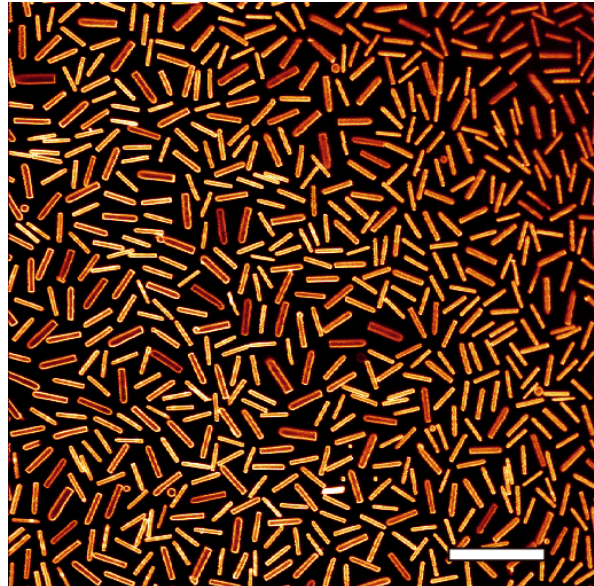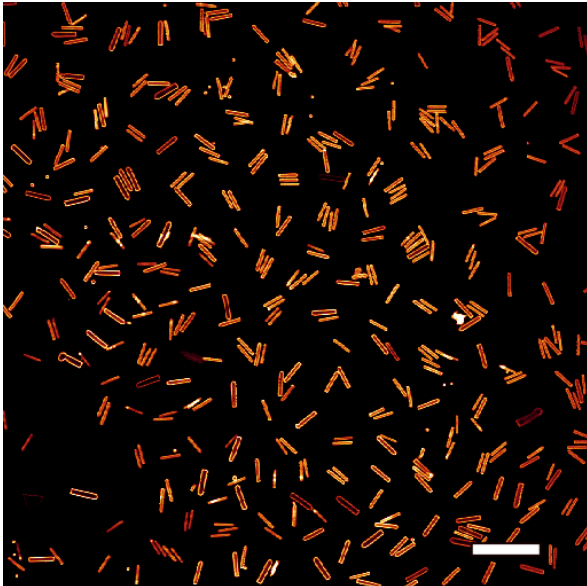## Towards a two-dimensional system

Tim Coopmans

Universiteit Utrecht

Supervisors

Thijs Besseling, Msc
Dr. Arnout Imhof
Prof. Dr. Alfons van Blaaderen

Abstract

We studied the phase behaviour of dilute systems of colloidal rods in electric fields by confocal microscopy. Sample cells with electrodes at the bottom and top of the sample were used. The first steps towards a two-dimensional systems of rods were taken. From a combination of theory and experiments, it was concluded that obtaining an experimental two-dimensional system of rods is probably possible, provided that sufficiently large rods are used. Also, new structures were seen: at certain concentrations, pair and cluster formation of rods at the bottom layer of samples, on an electrode, were observed. The corresponding attractive behaviour is not predicted in the theory of rods modelled by a string of induced point dipoles. A second layer on top of the bottom layer, consisting of rods which aligned with the electric field, is expected to turn the attraction into a repulsion. By constructing a phase diagram, we showed that the necessary conditions for pair and cluster formation are delicate. We obtained an experimental system of a single layer of rods aligned in the electric field, parallel to gravity. The study of such systems of colloidal silica rods not only provides insight in the fundamental interactions between polarized particles, but has many applications in e.g. calibration samples for new microscopy techniques and photonic crystals.

Contents

1 Introduction

Colloids, particles with sizes ranging from a few nanometers to several micrometers, are numerously present in everyday life. Mayonnaise, paint and blood are just some examples of colloidal systems. Not only can colloids be found in many substances that we use every day or in several applications such as electronic ink and photonic crystals, but they form a model system for the phase behaviour of smaller particles, such as molecules. Colloidal particles are small enough to move around in a random fashion due to thermal energy. This so-called Brownian motion is caused by the collision of the colloid with the molecules of its surrounding solvent. On the other hand, colloids are large enough to be imaged with today's microscopy techniques. The diffusion of molecules on large timescales can be modelled through the Brownian motion of colloids. In particular, the diffusion of rod-like molecules are of great importance in many biological and industrial processes. Also, many viruses have a rod-like shape. Lastly, knowledge of long molecules such as fats is desirable in the food industry. Not only insight in the mere Brownian motion of these rod-like particles is important, but ways to control this motion have great potential too. For example, the collective behavior of many rods under influence of an external electric field are of great use in many applications, not the least in the invention of the Liquid Crystal Display (LCD).

Much work on the dynamics and phase behaviour of rods has been performed already. It was observed that rods can form nematic, smectic, columnar and crystalline phases [1] [2]. Results of computer simulations of rods are in agreement with these observations [3] [4] [5]. Theory, computer simulations and experiments of both three-dimensional and two-dimensional systems of ellipsoids have been performed. However, an experimental two-dimensional system of rods has never been described in the literature, as opposed to ellipsoids [7].

The aim of this project is to study the behaviour of colloidal silica rods confined to two dimensions. A promising approach to this problem is through the use of electric fields. Kuijk et al. performed experiments with silica rods sedimented on an electrode [1]. With this electrode and another one on top of the dispersion of rods, an electric field was created. When the concentration was not too high, string formation of rods in the direction of the electric field was observed. The rods on the electrode, however, lied flat (see Fig. 1). This phenomenon was only observed when the electrode was on the inside of the cell. It was therefore expected to be a consequence of the formation of image charges in the electrode, which acts as a conducting plane. One of the objectives in this project is to find out whether it is possible to tune the concentration and electric field strength in order to obtain a system in which only the lying rods remain. In this way, a system of rods is obtained, in which the particles can freely move in the plane, but are confined in the z-direction by the force towards the electrode. It is our main aim to obtain such a two-dimensional system of rods.

The physics of a two-dimensional system of rods is very different from the three-dimensional variant, but not less rich. For example, no true long-ranged-order has been found and the isotropic-nematic phase transition is continuous [3]. The advantages of a two-dimensional systems lie in the experimental part: obtaining and analyzing confocal microscopy data is easier, as a two-dimensional system consists of a single plane and the orientation of rods can be described by a single angle only.

No suitable conditions for a two-dimensional system of rods confined by electric fields have yet been found in our experiments. Nonetheless, some new structures were found, such as the formation of pairs and clusters of rods, which indicate an unexpected attraction. In this thesis, we describe the efforts made in attempting to realize such a two-dimensional system.
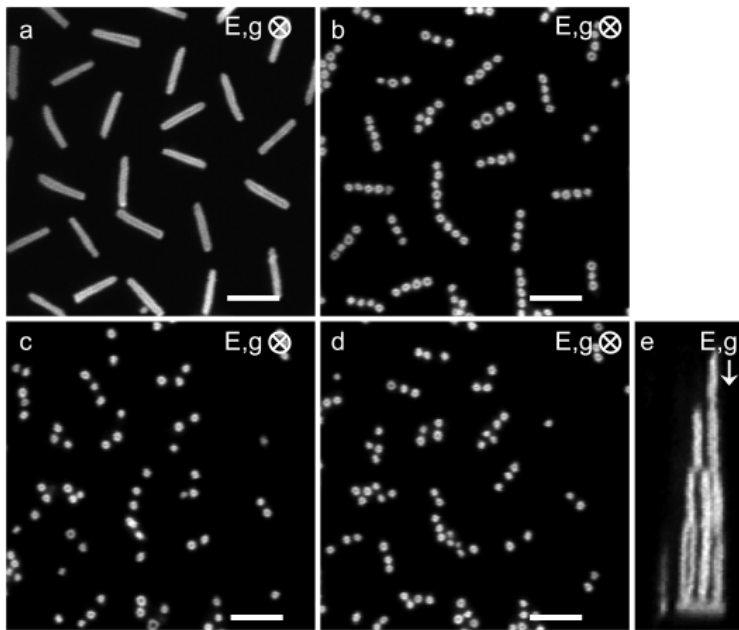
Fig. 1. Rods with aspect ratio $L/D = 6$ in a 0.5 V/μm, 1 MHz AC electric field, created by two parallel electrodes. Kuijk et al. showed that rods in an electric field aligned with the field, except for the rods lying on the electrode (Fig. (e)). A likely explanation for this is the induction of image charges in the electrode. Image a-d show the different layers in the z-direction. Scale bars indicate 5 μm. Reproduced from Kuijk et al. [1].

2 Theory

In this section, several models for polarizable rods in an electric field are described. The aim is to quantitatively understand why rods align with the external electric field and why some lie down on the electrode. We also aim to obtain quantitative expressions for interactions between the particles in an electric field.

To study the alignment of rods theoretically, we first approximate the spherocylindrical rod by an ellipsoid. Secondly, we explain the formation of strings of rods. Up to this point, we treat the rods as built up of fixed dipoles or charges. Because this is not a very accurate model of reality, we strengthen our hypotheses by modelling a single rod by two induced point dipoles. Using the same expressions, we calculate the interacting energy in a system of two inducible dipoles in an electric field. Lastly, we show the results of a numerical approach to the interaction between a rods and a conducting halfspace in an electric field. The combination of all of these results gives us a firm theoretical background to understand interactions in systems of rods.

2.1 The ellipsoid model for one rod in an electric field

It is known that the polarization induced in a colloid in an external electric field can be approximated by an induced dipole positioned in the colloid, provided that the dielectric constant of the colloid does not differ too much from that of the surrounding solvent and the external electric field strength is not too high [1]. Although the induced dipole moment in spheres and ellipsoids can be calculated analytically, only numerical values for this exist for spherocylinders (cylinders with hemispheres on the ends). Fortunately, Venermo and Sihvola have shown in a numerical study that the dielectric polarizability of cylinders differs not more than 10% form the polarizability of ellipsoids of the same volume and aspect ratio [6]. We may therefore expect that taking an ellipsoid as a model for our spherocylinders would make a reasonable approximation to the induced polarization in our rods.

The dipole moment of an ellipsoid is given by

$$p_i = \alpha_i \epsilon_s V E_i \text{ with } \alpha_i = \frac{\epsilon_c - \epsilon_s}{\epsilon_s + N_i(\epsilon_c - \epsilon_s)} \tag{1}$$

where i denotes the axis of the ellipsoid, ϵ_s the dielectric constant of the solvent, ϵ_c the dielectric constant of the colloid, V the volume of the colloid, E_i the external electric field and N_i the depolarization factor.

The depolarization factor gives information about the weakening of the polarization on the internal field within the ellipsoid. If the depolarization factor is zero, the internal electric field is the same as the external electric field. For ellipsoids, it is known that the depolarization factors are given by [6]:

$$N_x = \frac{1 - e^2}{2e^3}(\text{Log}[\frac{1+e}{1-e}] - 2e) \tag{2}$$

$$N_y = N_z = \frac{1}{2}(1 - N_x) \tag{3}$$

where $e = \sqrt{1 - \frac{a_y{}^2}{a_z{}^2}}$ is the eccentricity and a_i the semi-axis of the ellipsoid. We have chosen the long axis to be in the x-direction.
The potential energy of a dipole in an electric field is given by

$$U = -\vec{p} \cdot \vec{E} \tag{4}$$

so U is minimal if $\vec{p}$ is parallel to $\vec{E}$. Because the polarizability α_i is largest in the x-direction (in the ellipsoid-frame), U will be minimal if $\vec{p}$ and $\vec{E}$ are in the x-direction (in the ellipsoid-frame). We draw the conclusion that the ellipsoid aligns with the electric field. Using this model, we expect individual spherocylinders, far away from the electrode and in a homogeneous electric field, to align with the electric field as well.

7

2.2 Static models for interacting rods in an electric field

2.2.1 String formation of rods

In the ellipsoid model, the influence of the electric field on a single particle was studied. This approximation only holds for very dilute suspensions. When the concentration increases, the particles start to interact with each other via their induced dipole moments. We now model the dipole moment of the polarized rods by two equal charges located in the ends of the rods. Polarization of one of the rods by the electric field of the other is neglected.

In the ellipsoid model, rods are expected to align with the field. Upon increasing the concentration, two rods come closer together. We calculate the difference in potential energy in two configurations (see Fig. 2): (A) with two rods parallel next to each other and (B) with two rods placed head-to-toe. The energy difference is given by [8]

$$\Delta U = U_A - U_B = \frac{1}{4\pi\epsilon_0\epsilon_s} \sum_{i=1}^{4} \sum_{j>i}^{4} q_i q_j \left(\frac{1}{r_{ij,A}} - \frac{1}{r_{ij,B}} \right). \tag{5}$$

Working out this expression for the situations in Fig. 2, we obtain

$$\Delta U = \frac{q^2}{4\pi\epsilon_0\epsilon_s} \left(\frac{3}{D+x} - \frac{2}{L+x} - \frac{2}{\sqrt{(D+x)^2 + (L-D)^2}} + \frac{1}{2L+x-D} \right). \tag{6}$$

As ΔU is positive, string formation is energetically favorable.
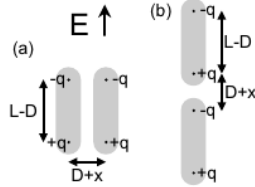

Fig. 2. Model in which two opposite charges, placed at relative distance $L - D$ represent the dipole in the rod. The distance x was introduced to accommodate the electric double layer. Reproduced from Kuijk et al. [1]

2.2.2 Two fixed parallel point dipoles at an angle

We want to confirm that string formation is also energetically favorable in the situation of two rods modelled by two fixed parallel point dipoles. We take two parallel, equal dipoles placed with a relative distance vector $\vec{r} = \vec{r}_2 - \vec{r}_1$. Their dipole moments make an angle θ with the line connecting the dipoles, as indicated in figure 3. The interaction energy of two dipoles is given by

$$U = \frac{1}{4\pi\epsilon_0\epsilon_s r^3} [\vec{p}_1 \cdot \vec{p}_2 - 3(\vec{p}_1 \cdot \hat{r})(\vec{p}_2 \cdot \hat{r})] \tag{7}$$

[8] which for two fixed parallel and equal point dipoles becomes

$$U = \frac{1}{4\pi\epsilon_0\epsilon_s r^3} [p^2 - 3(\vec{p} \cdot \hat{r})^2] = \frac{p^2}{4\pi\epsilon_0\epsilon_s} \frac{1 - 3\cos^2(\theta)}{r^3} \tag{8}$$

which changes sign at $\theta = \arccos(\frac{1}{3}\sqrt{3}) \approx 54°$. In words, this means that two parallel dipoles, separated at an arbitrary distance, attract each other for $\theta > 54°$ and repel each other for $\theta < 54°$.

Fig. 3. Model of two rods as fixed parallel (mathematical) dipoles. The connecting line between the positions of the dipoles makes an angle θ with the direction of the dipoles.

In conclusion, these models predict that rods align with the electric field, and attract each other when the angle between their connecting line is large enough. So when a rod gains enough height by thermal motion and the electric field is directed parallel to gravity, it is energetically favorable to position itself head-to-toe with a neighboring rod. Thus strings are formed.

2.3 Interacting induced dipoles in an electric field

In the models in the previous section, we used dipoles with fixed dipole moment. To obtain a more accurate description of a suspension of rods, we model a rod by two dipoles, positioned at position $\vec{r_1}$ and $\vec{r_2}$, whose electric fields influence each other [9]. A schematic view of this model is pictured in Fig. 4. We have two equations to solve:

$$\vec{p_1} = \alpha_1 \vec{E}_{loc,1} = \alpha_1(\vec{E}_0 + \vec{E}_2(\vec{r_1})) \tag{9}$$

$$\vec{p_2} = \alpha_2 \vec{E}_{loc,2} = \alpha_2(\vec{E}_0 + \vec{E}_1(\vec{r_2})) \tag{10}$$

where α_i is the polarizability of dipole i, $\vec{E}_0$ the applied external field, $\vec{E}_{loc,j}$ the local electric field at position $\vec{r}_j$ and $\vec{E}_k$ the electric field of the dipole k.
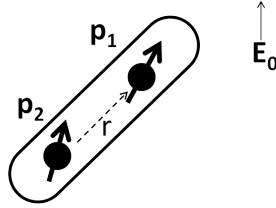

Fig. 4. Model of a single rod as two inducible dipoles, with relative distance vector $\vec{r}$. The rod is placed in an external electric field.

We know that the electric field of one dipole at the position of the other is given by

$$\vec{E}_1(\vec{r_2}) = M(\vec{r_2} - \vec{r_1}) \cdot \vec{p_1} \tag{11}$$

where the matrix M is given by

$$M(\vec{r_2} - \vec{r_1}) = \frac{1}{4\pi\epsilon_0\epsilon_s}\left(\frac{3(\vec{r_2} - \vec{r_1})(\vec{r_2} - \vec{r_1})}{|\vec{r_2} - \vec{r_1}|^5} - \frac{I}{|\vec{r_2} - \vec{r_1}|^3}\right) \tag{12}$$

with I the identity matrix [8]. Furthermore, we use the notation of a matrix by two vectors, in which the entries of the matrix are defined by $(\vec{a}\vec{b})_{ij} = a_i b_j$.

Via symmetry and the fact that $\vec{\nabla} \times \vec{E} = \vec{0}$, one obtains

$$M = \frac{1}{4\pi\epsilon_0\epsilon_s r^3}(3\hat{r}\hat{r} - I), \tag{13}$$

where $\hat{r} := \frac{\vec{r_2} - \vec{r_1}}{|\vec{r_2} - \vec{r_1}|}$. Using all of above, the equations to solve become

$$\vec{p_1} = \alpha_1(I - \alpha_1\alpha_2 M^2)^{-1} \cdot (I + \alpha_2 M) \cdot \vec{E}_0 \tag{14}$$

$$\vec{p_2} = \alpha_2(I - \alpha_1\alpha_2 M^2)^{-1} \cdot (I + \alpha_1 M) \cdot \vec{E}_0. \tag{15}$$

Now p_1 and p_2 can in principal be calculated. For equal rods we have equal polarizability ($\alpha_1 = \alpha_2 = \alpha$). The solution to equation (15) then becomes

9

$$\vec{p_1} = \vec{p_2} = [\alpha_\perp (I - \hat{r}\hat{r}) + \alpha_{||}\hat{r}\hat{r}] \cdot \vec{E_0} \tag{16}$$

with

$$\alpha_\perp = \frac{\alpha}{1 + \frac{\alpha}{4\pi\epsilon_0\epsilon_s r^3}} \tag{17}$$

$$\alpha_{||} = \frac{\alpha}{1 - \frac{\alpha}{2\pi\epsilon_0\epsilon_s r^3}} \tag{18}$$

Now if we model an initially unaligned rod by two induced point dipoles, as pictured in figure 4, $\hat{r}$ has a nonzero angle with $\vec{E_0}$. By equation (16), the dipole moment of any of the two point dipoles, $\vec{p}$, has a nonzero angle with $\vec{E_0}$ too. Therefore there is a torque $\vec{\tau} = \vec{p} \times \vec{E_0}$ on the rod. This torque results in alignment of the rod with the electric field. In conclusion, this more accurate model of a rod predicts alignment too. Also, we see that the torque is proportional to the electric field strength: $\tau = pE_0\sin(\phi)$ where ϕ is the angle between $\vec{p}$ and $\vec{E_0}$. For a rod to overcome the gravitational force in the case that the electric field is directed parallel to gravity, the torque must be sufficient. Whether this is the case, depends on the angle of the semi-axis of the rod with $\vec{E_0}$ and on the electric field strength, E_0. Therefore: the higher the electric field, the more rods align with the field.
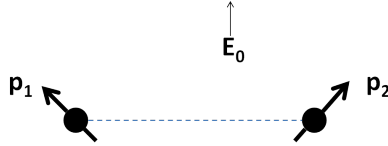

Fig. 5. Model of two rods as two inducible dipoles (i.e. their dipole moments influence each other). The electric field is perpendicular to the line connecting their positions.

2.4 Building up a rod of many dipoles and introducing the electrode

Kwaadgras et al. modelled rods by a string of six inducible dipoles, as schematically drawn in Fig. 6 [10]. They calculated the potential energy of a single rod at a variable angle θ with respect to an external electric field and is positioned at a distance h from a conducting halfspace. The electric field direction is perpendicular to the conducting halfspace. The results are shown in Fig. 7. From the graphs it is clear that it is energetically favorable for a rod to align with the electric field. That is, have $\theta = 0$, at the global minimum. However, there is a local minimum for $\theta = \frac{\pi}{2}$, when the rod is close enough to the conducting halfspace. Also, the maximum shifts to higher θ for increasing distance h between the rod and the halfspace. The initial height and angle of the rod before turning on the electric field determines its angle afterwards: either standing up ($\theta = 0$, in the global minimum) or lying down ($\theta = \frac{\pi}{2}$, in the local minimum). The motion of the rod at the moment when the electric field is turned on and its speed of polarization play a role too in determining which minimum the rod will end up in.

For $h = 0$, the maximum of the potential energy is close to $\theta = \frac{\pi}{2}$ and it moves toward $\theta = \frac{\pi}{2}$ upon increasing the distance h between the rod and the plane. It is therefore expected that large rods only, that have a high tendency to lie flat and can gain only little height due to thermal motion, will end up in the local minimum at $\theta = \frac{\pi}{2}$.
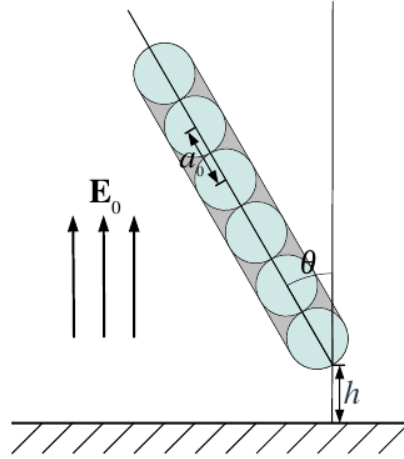
Fig. 6. Schematic drawing of the model of a single rod, built up of six inducible dipoles, used by Kwaadgras et al. The rod has a angle θ with respect to the external electric field and is positioned at a distance h from this halfspace.
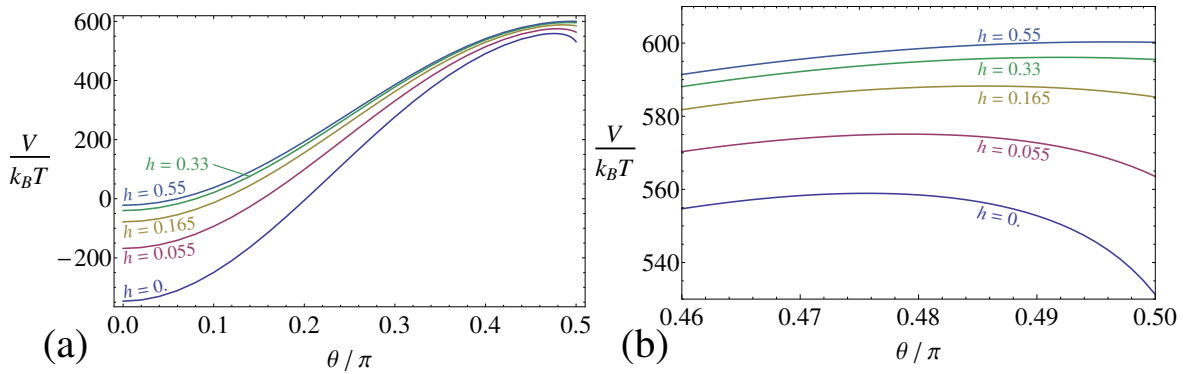

Fig. 7. Calculation of the the potential energy of a rod as a function of the distance to and its angle with a conducting plane. The applied field is $E_0 = 0.3$ V/μm, the distance to the plate h is given in μm and the polarizability of each of the dipoles of the rod is 0.03 μm^3. These values roughly match the rods used in our experiments (B35-rods), as described in section 3. For the chosen parameters, the well at $\theta = \frac{\pi}{2}$ is about 30 k$_b$ T deep.

Kwaadgras et al. calculated the potential energy of a system of two parallel lying rods as well. Again, a rod is modelled as six inducible dipoles. A first rod is placed lying down on the conducting halfspace. A second rod is positioned lying on the halfspace too, parallel to the first rod. The distance between the two rods and angle of the line connecting their center-of-mass are varied. The result is shown in Fig. 8. The potential energy decreases for increasing distance in any configuration of the two parallel rods, so the force between the rods is repulsive. We therefore do not expect a parallel pair of two parallel rods close to each other, to be formed. [11].
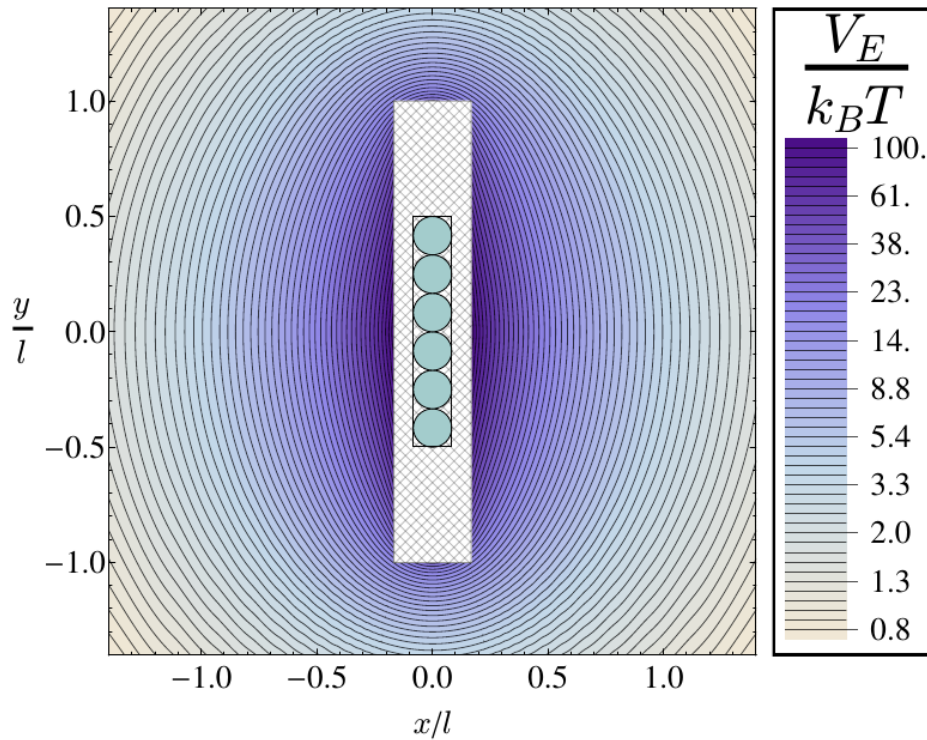
Fig. 8. The potential energy of a system of two parallel rods, lying on a conducting halfspace. A configuration with a first rod fixed in the origin, and a second rod, parallel to the first, was used. The potential energy of the second rod as a function of its center-of-mass has been drawn as a contour plot [11]. It can be seen that the potential energy decreases with increasing distance between the rods, corresponding to a repulsive force in any configuration.

2.5 Summary

In conclusion, both our models for a single rod (a rod as a fixed dipole, as an ellipsoid, as built up of two inducible dipoles and a rod near a conducting plane) and for two rods (two single inducible dipoles) explain why rods align with an applied the electric field. Also, string formation follows from the theory. The fact that some rods in an electric field near a conducting plane lie down has been elucidated. Lastly, the force between two parallel rods lying down on an electrode is calculated to be repulsive.

All of our models predict repulsion between two aligned rods on the bottom (not on top of each other).

# 3 Observations of rods in a single electric field

3.1 Experimental setup

Particles

In our experiments we used two types of silica rod-like particles of a few micrometers in size (see Table 1). The particles were shaped like a bullet, with a flat and a rounded end. The B35-rods consisted of a non-fluorescent core of 230 nm, a fluorescent FITC shell of 30 nm thick and a 190 nm non-fluorescent outer shell. The MS1-rods were constructed likewise, but are dyed with rhodamine isothiocyanate (RITC) instead of fluorescein isothiocyanate (FITC).[1].
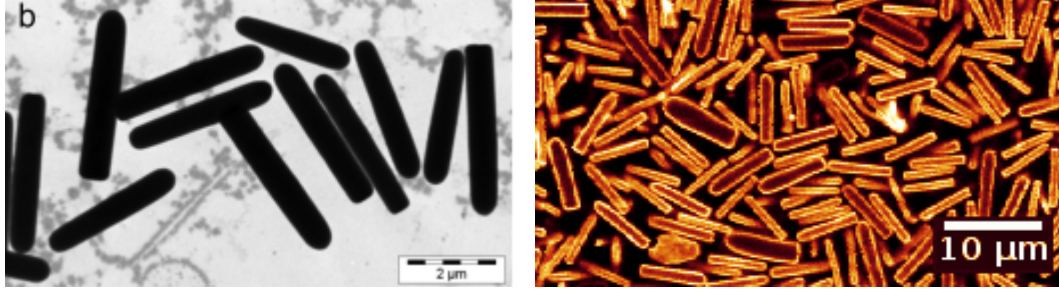
(a) TEM-image of B35-rods [1].

(b) Confocal microscope image of MS1-rods. Polydispersity is larger than 10%.

Fig. 9. Images of the used B35-rods ($L = 3.3$ μm and $D = 0.550$ μm as measured with TEM) and MS1-rods ($L = 5.7$ μm and $D = 1.1$ μm as measured with confocal microscopy).

Dispersion

We dispersed the rods in a mixture of dimethylsulfoxide (DMSO, refractive index $n_D = 1.48$) and water ($n_D = 1.33$). The particles have a refractive index of $n_D = 1.45$. We used a mass ratio of DMSO and water of 10:1 so that the mixture had approximately the same refractive index as the particles. As a consequence of this refractive index matching, not only Van der Waals interactions will be minimalised, but the amount of light scattered in confocal microscopy (see section 3.1.1) will be reduced too.

Diffusion

The rods move around in a random fashion in the solvent due to Brownian motion. The two-dimensional diffusion of a rod over an average distance and angle are given by

$$< r^2 >= 4D_t t, \qquad < \theta^2 >= 2D_\theta t \tag{19}$$

where t is the time needed for the diffusion over a distance r or an angle θ, and D_t and D_θ are the translational and rotational diffusion coefficients, respectively. For rods, modelled as cylinders, these diffusion coefficients are given by [1]

$$D_t = \frac{k_B T(\text{Log}(\frac{L}{D}) + v)}{3\pi\eta_0 L}, \qquad D_\theta = \frac{3k_B T(\text{Log}(\frac{L}{D}) + \delta_\perp)}{\pi\eta_0 L^3}. \tag{20}$$

where k_B is Boltzmann's constant, L the head-to-tail length of the rod, D the diameter of the rod and η_0 the viscosity of the solvent. The terms v and $\delta_\perp$ are necessary to include end-effects. For short rods ($2 < \frac{L}{D} < 30$), these are [1]

$$v = 0.312 + 0.565\frac{D}{L} - 0.100(\frac{D}{L})^2, \qquad \delta_\perp = -0.662 + 0.917\frac{D}{L} - 0.050(\frac{D}{L})^2. \tag{21}$$

For our samples, the solvent is a mixture of DMSO and water, which has a viscosity of 1.9 mPs. With equation 19, the time t_L needed for a rod to diffuse over a distance equal to its length and the time t_π needed to diffuse over an angle π can be calculated. They are shown in Table 1.

---

[1]Information on the synthesis and more information on the properties of the B35-rods can be found in [1] and [12].

13

Name	L (μm)	σ_L	D (μm)	σ_D	L/D	Fluorescent dye	V (μm^3)	L_g(μm)	t_L (s)	t_π (s)
B35 [1]	3.3	10%	0.550	11%	6.0	FITC	0.74	0.7	18.1	67.9
MS1	5.7	>10%	1.1	>10%	5.2	RITC	5.07	0.1	99.1	386.9

Tab. 1. Properties of silica rod-like particles used, with length L, diameter D, volume V and gravitational length L_g at room temperature ($T = 293$ K). The polydispersity in length is defined as $\sigma_L = \frac{\delta_L}{<L>}$ where δ_L is the standard deviation in length of the particles. The sizes of the B35-rods were measured with TEM, the sizes of MS1-rods with confocal microscopy. The gravitational length is given by $L_g = \frac{E_{thermal}}{mg} = \frac{k_b T}{mg}$ with k_b Boltzmann's constant, T the absolute temperature, m the mass of the particle and g the gravitational acceleration on earth. It is the height a particle with an energy of 1 $k_b T$ can gain.

Electric cell

In order to research the behaviour of the particles in a single electric field, we used sample cells (shown in Fig. 10), with two conductive indium tin oxide (ITO) coated glass slides (conductivity 30-60 Ω/Sq, supplier Diamond Coatings Ltd.). We used cells with the coated part on the inside of the cell (in contact with the suspension) as well as on the outside. These coated glass slides were separated by glass spacers of a thickness of approximately 100 μm (No. 0, by Menzel-Gläser). The components were glued with UV-glue (Norland No. 68). Using silver paint (SPI #0005), thermocouple alloy wires (diameter 50 μm, supplier Goodfellow Cambridge Ltd.) were glued to the coated part of the glass slides. The cells were either sealed by either UV-glue only, or first by candle wax and then by UV-glue on top of the wax, because UV-glue reacts with DMSO, as described in appendix A.
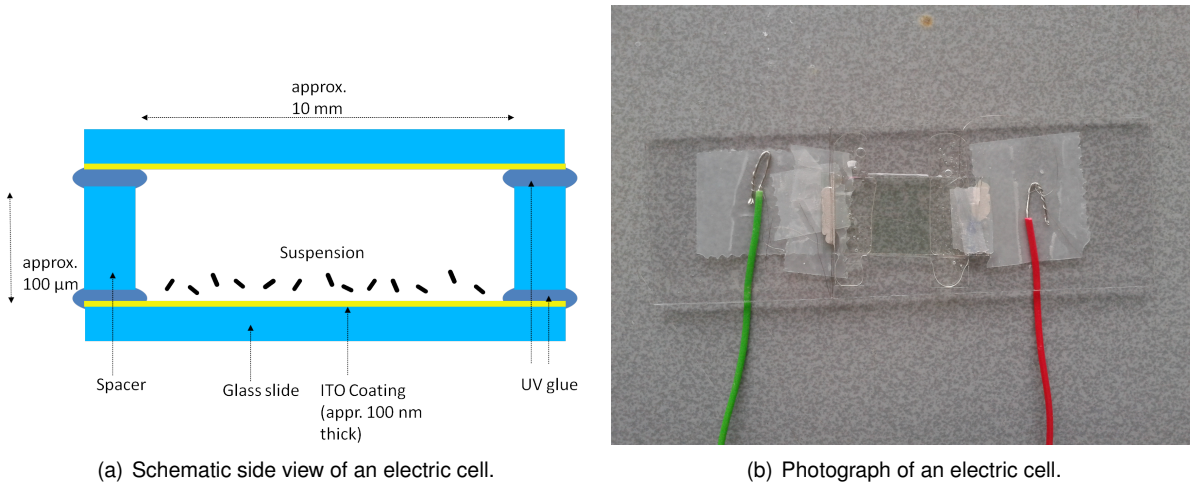

(a) Schematic side view of an electric cell.

(b) Photograph of an electric cell.

Fig. 10. Images of a cell used to put a homogeneous electric field over a dispersion of rods.

Electric field

We used a voltage generator (Agilent, type 33120A) to generate a (sinusoidal) signal with an amplitude of 2.0 Volts (peak-to-peak) and a frequency of 1 MHz. The signal from the voltage generator was sent to a wide band amplifier (Krohn-Hite, type 7602M). The amplifier was connected to the sample as described above.

We apply an alternating current (AC) electric field. As theory (section 2.3) predicted that a spherocylinder aligns in a constant electric field, the torque on the rods, $\vec{\tau} = \vec{p} \times \vec{E}$, does not change in an AC-field: when the direction of the current switches, $\vec{E}$ does as well. As $\vec{p}$ aligns with $\vec{E}$, $\vec{p}$ changes its direction too and the alignment torque $\vec{\tau} = (-\vec{p}) \times (-\vec{E}) = \vec{p} \times \vec{E}$ on the particle remains the same. Moreover, using an alternating current instead of direct current (DC) gives the advantage that ions in the solvent will not move so that electrohydrodynamics is minimalised, nor will electrolysis take place, provided the frequency of the AC is high enough. A frequency of 1 MHz, which was used in our experiments, is sufficient to prevent this.

The electric field strength in cells with the electrodes (coated part of the glass) on the inside is

$E = V/d$ where V is the applied voltage difference and d the distance between the coated glass slides. For cells with the electrodes on the outside, the field strength in any of these layers can be calculated with:

$$E_i = \frac{V}{\epsilon_i} \frac{\epsilon_1 \epsilon_2 \epsilon_3}{(d_1 \epsilon_2 \epsilon_3 + d_2 \epsilon_1 \epsilon_3 + d_3 \epsilon_1 \epsilon_2)} \tag{22}$$

where ϵ_i is the dielectric constant of the material the electric field strength is calculated in, ϵ_{1-3} the dielectric constant of layer 1-3 and d_{1-3} the thickness of layer 1-3. For our cells, with two layers of glass ($\epsilon = 3.5$ and $d = 100\mu m$) and solvent (DMSO/water) in between ($\epsilon = 50$ and $d \approx 100\mu m$), the electric field strength becomes $E = 3.4 \cdot 10^{-4} \cdot V$ in $V/\mu m$ [1].

3.1.1 Imaging by confocal microscopy

The rods were made visible by confocal laser scanning microscopy (CLSM). All confocal microscopy measurements were performed with a Leica SP2 or Nikon C1 confocal microscope, except for the images in section 5, which were made with a Leica SP8 confocal microscope. A schematic overview of the principles of a confocal microscope is given in Fig. 11. Laser light is directed by a dichroic mirror through an objective lens. There the laser light excites the dye molecules (FITC or RITC) in the particles in our sample. The light that comes off this excitation returns through the same lens and passes through a dichroic mirror, where it falls into a photomultiplier tube (PMT). In the PMT the signal is amplified. Just before reaching the PMT, the light passes through a pinhole. All light from the focal plane can pass through the pinhole, but most light from other parts of the sample cannot. This pinhole therefore increases resolution in comparison with conventional microscopical imaging. The resulting fluorescent light is then redirected towards a scanner. The resolution of our images is approximately 250 nm in the plane and 750 nm along the optical axis (in the z-direction).
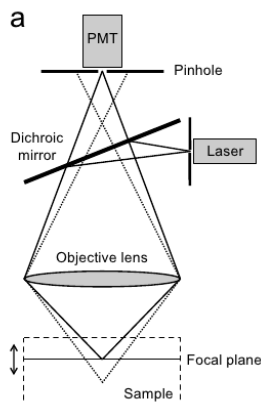

Fig. 11. The operating principle of a confocal microscope. Image reproduced from Kuijk et al [1].

3.1.2 Particle tracking

In order to accurately obtain the position of rods from the confocal microscope images, two computer programs written by Besseling and Hermes were used [13]. The first computer program can identify the positions of spherical particles in confocal microscope images. This program was used to analyze images of standing rods viewed from below. The second computer program can identify the position, orientation and length of lying rods, viewed from below. The algorithm of these programs is similar to the method described by Crocker and Grier[14], but extended to 3D as *e.g.* schematically described in [15].

15

3.2 Results

3.2.1 Distribution of the angle between rods and an external electric field

Information of the tendency of the rods on the electrode to align with the electric field is valuable in view of our aim to obtain a two-dimensional system of lying rods. For this reason, the distribution of the angle between rods on an electrode and the electric field perpendicular to this electrode was measured. The position, orientation and length of B35-rods in confocal microscope images were identified using the tracking algorithm for rods, as described in section 3.1.2. An example of a confocal microscope image of B35-rods on an electrode and the identification of these rods is shown in Fig. 12. A rod visible in a confocal microscope image is in fact the projection of the length of this rod in the xy-plane. The angle between a rod and the electric field can be calculated from this projection length and its actual length. From the confocal images of B35-rods on an electrode, the distribution of these angles θ in the presence and in the absence of an electric field were obtained. This distribution is shown in Fig. 13. The tracking program slightly overestimates the length of the aligned rods (viewed as spheres from below). Therefore, the small angles of rods with the electric field will be overestimated as well.
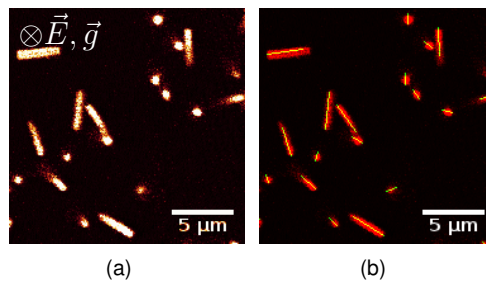

(a)   (b)

Fig. 12. (a) Confocal microscope image of B35-rods on an electrode in a 0.015 V/μm, 1 MHz electric field. A computer program was used to identify the projective length of the rods in the xy-plane, described in section 3.1.2. The result of this identification is shown in Fig. (b). It can be seen that the program overestimates the length of the aligned rods (spheres as viewed from below), corresponding with a overestimation of the angle between the rods and the electric field when the angle is small.

The difference in the histograms in Fig. 13 for rods with and without an external electric field is the peak for angles below 0.06 rad. when the electric field is turned on. This indicates that a high fraction of rods aligns with the electric field, which is in agreement with the broad well around the global minimum at $\theta = 0$ in the calculations of Kwaadgras et al. as described in section 2.4. The well around the local minimum $\theta = \frac{1}{2}\pi$ in the calculations of Kwaadgras et al. is very small, so much statistics is needed to experimentally verify the existence of this local minimum. As the histogram for rods in an electric field does not show a peak in the fraction of rods lying down on the electrode (with $\theta \approx \frac{1}{2}\pi$), no conclusions about this local minimum can be drawn from these measurements. However, from the fact that less than 3% of the rods have $\theta > 0.4\pi$, we may conclude that only a small fraction of the rods lies down on the electrode.

The fact that both histograms decrease in fraction of rods for high angles ($\theta > 0.3\pi$, approximately) is probably caused by height gain of the rods due to thermal motion. When a rod has 1 k_bT of thermal energy, its center of mass can move up to its gravitational length in height, which is 0.7 μm in case of the B35-rods. This corresponds to an angle between the rod an the electrode of $\theta = \arccos(\frac{L_{gravitational}}{\frac{1}{2} \cdot L}) = \arccos(\frac{0.7}{\frac{1}{2} \cdot 3.3}) \approx 0.36\pi$. Indeed, both histograms have a negative slope for $\theta > 0.36\pi$.
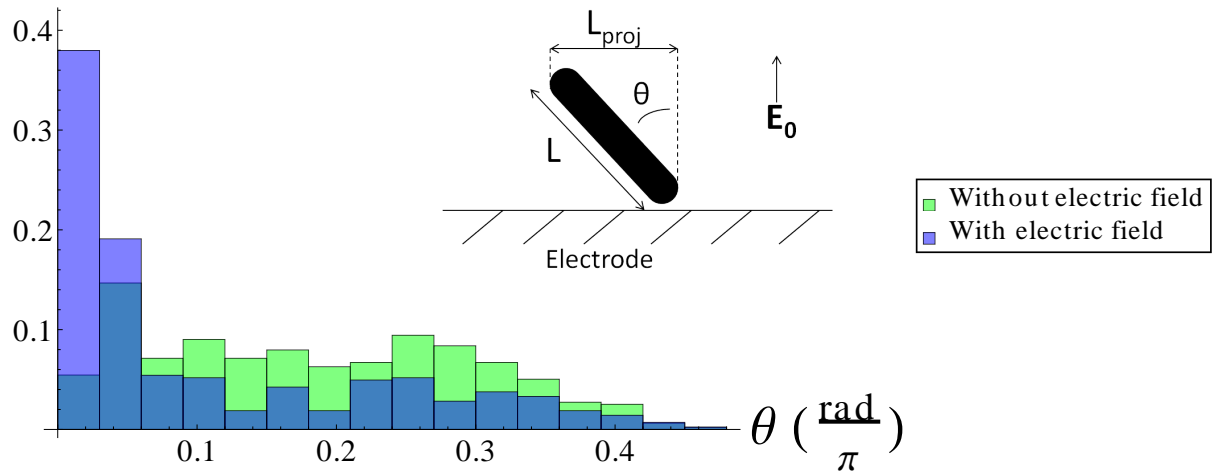
Fig. 13. Histograms from experimental observations of the angles between the orientation of B35-rods and a line perpendicular to the electrode, in the presence and the absence of an electric field. The main difference between the histograms is the peak for small angles θ for rods with an electric field, indicating a strong tendency to align with the electric field. The negative slope for $\theta > 0.3\pi$ approximately of both histograms is probably caused by thermal motion in height, as explained in the text. The histogram for rods in the presence and absence of an electric field is constructed from data from 424 and 477 rods, respectively.

3.2.2 Pair formation

At low volume fraction, a new structure was observed when an electric field was present: pairs of parallel rods lying on the electrode were formed (see Fig. 14a). Also, more complicated structures were formed, such as squares (Fig. 14a, on the left), and pentagons (Fig. 14b). All observed structures (pairs, triangles, squares etc.) disappeared immediately when turning off the electric field. The observed attraction is therefore probably caused by the external electric field. The formation of triangles, squares and more complicated figures are likely explained by emulsion droplets of glue on the bottom of the sample. These emulsion droplets are a consequence of the reaction of the solvent (DMSO) with the UV-glue, as described in appendix A. It is expected that the rods are attracted to the emulsion droplets when turning on the electric field, resulting in rods surrounding a droplet (that is invisible in the fluorescence images). Thus a triangle (three rods around a droplets), square (four rods) and more complex figures are formed. Also, the attraction might partially be induced by a depletion interaction, caused by drops of glue, acting as a depletent.

It was observed that the single rods lying down had rods standing on top of them, which together make the same 'flats' of rods observed by Kuijk et al, as shown in Fig. 1. However, most pairs of rods did not.
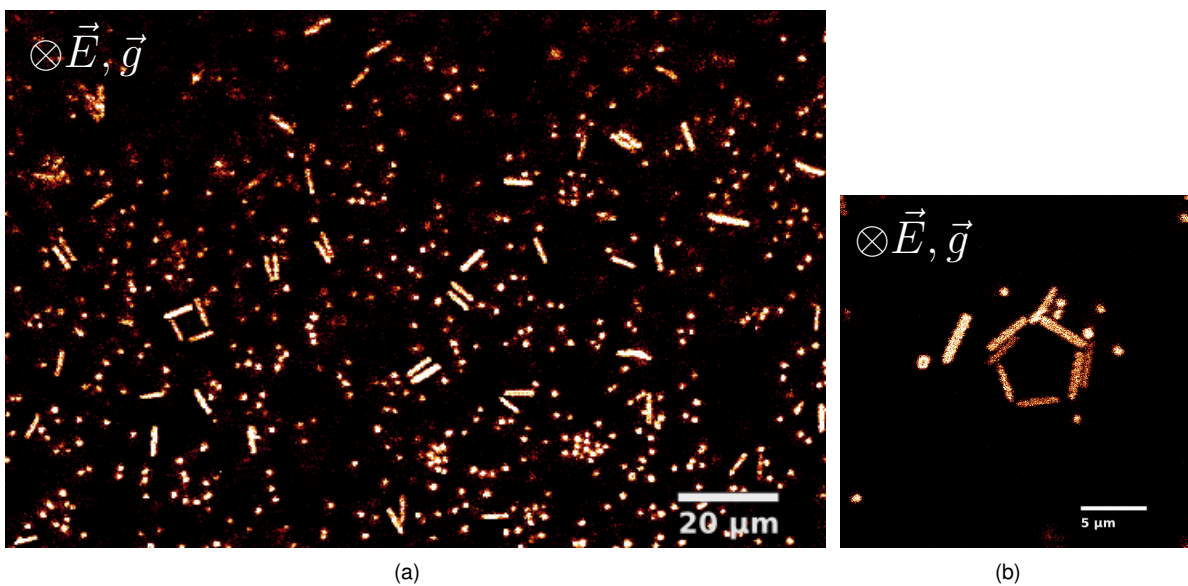

(a) (b)

Fig. 14. Confocal microscope image of B35-rods in an electric field of 0.011 V/μm. The rods lie on an electrode. Some of them form pairs. Even more complicated figures were observed such as (a) squares and (b) pentagons. Images were taken in the middle of the sample, approximately one hour after preparation.

To find out whether this pair formation was a consequence of the closeness of the electrodes, an electric cell with the electrodes on the outside of the cell was used. Again, this pair formation was observed (see Fig. 15). Clusters of three or more rods were seen as well.

Fig. 16 shows two rods sedimented on glass, with an external electric field. They stay together for at least 7 minutes. This strongly indicates an attraction. However, the attraction of the particles seems to be less than when the particles are in direct contact with the electrode, as observed by eye. This "floppiness" of these pairs (such as in Fig. 16) indicates that the interaction energy is of the order of their thermal energy, a few k_bT.
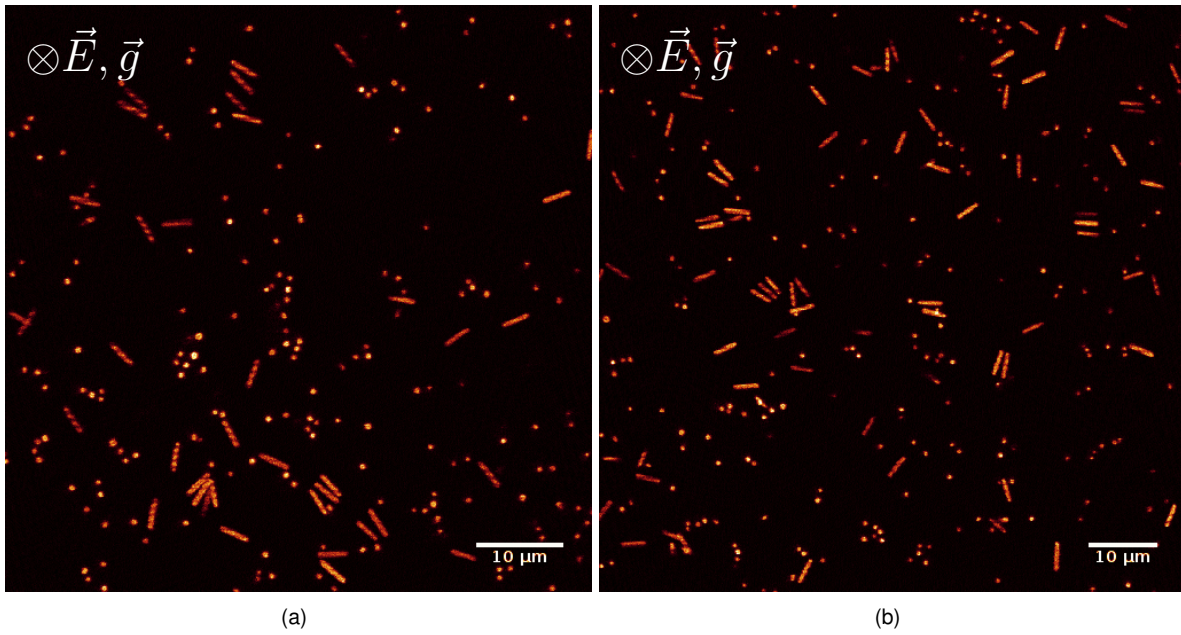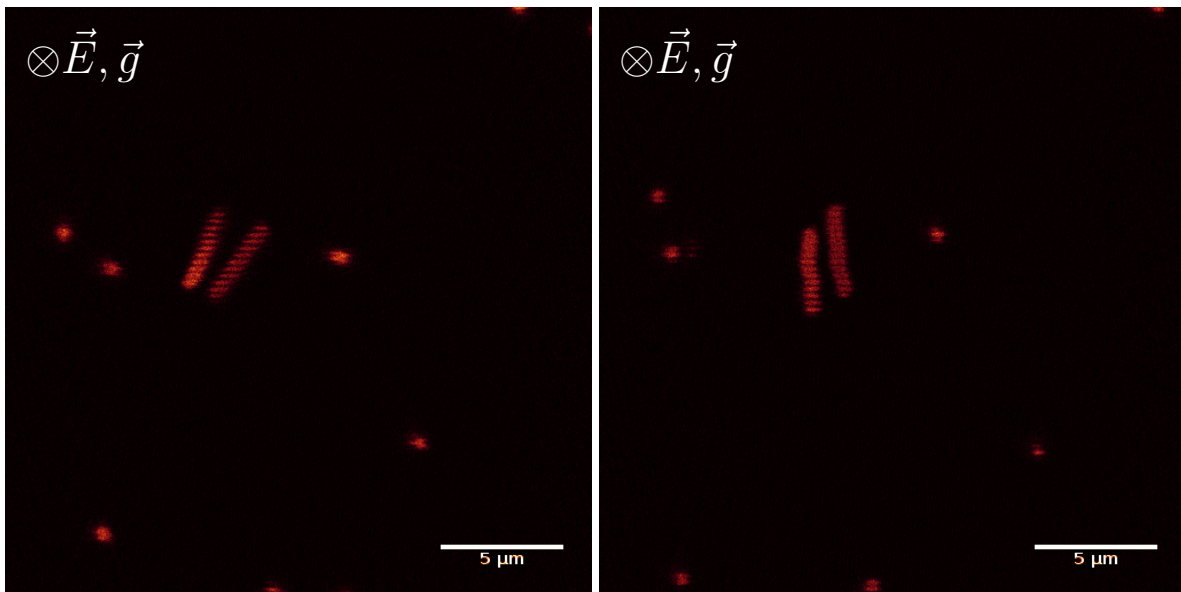
18

(a)

(b)

Fig. 15. Typical pictures of pairs of B35-rods in a cell with the electrodes on the outside (rods cannot come into contact with the electrode). The electric field strength was 0.032 V/μm. Images were taken in the middle of the sample, approximately one hour after preparation.

(a) A pair of B35-rods in a 0.032 V/μm electric field in a cell with the electrodes on the outside (the particles are separated from the electrode by a 100 μm layer of glass). Image was taken in the middle of the sample, approximately one hour after preparation.

(b) The same pair, 7 minutes later.

Fig. 16

### 3.2.3   Influence of concentration on attraction between particles

Another structure not seen before experimentally was observed. Fig. 17 shows MS1-rods in an electric field, lying on an electrode, exhibiting attracting behaviour. We observed that the structures that were caused by the attractions are dependent on concentration. We distinguish between four different ranges of concentration. The bottom layer of these different concentrations (rods on the electrode) is imaged in Fig. 17).

(a) Very dilute suspension. Rods do not stand on top of each other, nor is there any interaction clearly visible. We observe rods standing up (i.e. aligning with the field) as well as lying down on the electrode.

(b) Dilute suspension, for which we observe the formation of pairs. Also, we see more complex figures such as triangles and squares of rods. Again, we see rods standing up and lying down, but rods do not stand on top of each other.

(c) Semi-concentrated suspension, with cluster formation. The clusters mainly consist of three or four rods. The figure shows the bottom layer: on these clusters some rods standing up as well as lying down are observed. Also, the clusters seem to repel each other. Fig. 18 shows that (1) clusters have a lot of rods on top and (2) rods standing up on the endpoints of two rods lying down seem to prevent the lying ones from pair formation.(3) We also observed T-shaped pairs of rods, where the touching point of the bars in the letter 'T' is exactly the point where the vertical rod stands.

(d) Concentrated suspension, with almost only rods lying down. The figure shows the bottom layer. On top of this we have a single layer of rods standing up. From the figure it can be seen that the flats as a whole exhibit a repulsive interaction, which can be explained by the induction of dipoles in the length of the rods. The behaviour at this concentration resembles the 'flat formation' of rods observed by Kuijk et al [1]. However, their images show a far more dilute bottom layer, which can be explained by the fact that the MS1-rods are much larger than the B35-rods used by Kuijk et al. (see section 3.1 for details on the sizes of B35- and MS1-rods). Also, some smectic-like rows of the bottom rods of these 'flats' were observed, but after 45 minutes, there was still no definite ordering in the bottom layer.
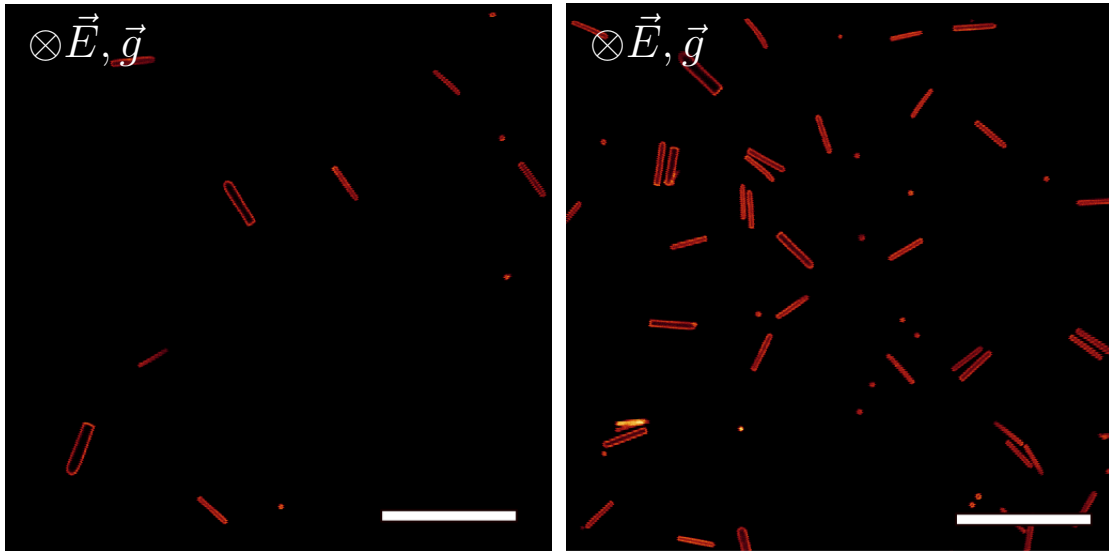
(a) Very dilute suspension, with both rods lying down and standing up. No attraction is visible.

(b) Dilute suspension, with both rods lying down and standing up. Pairs of parallel rods are observed. No rods stand on top of these pairs.
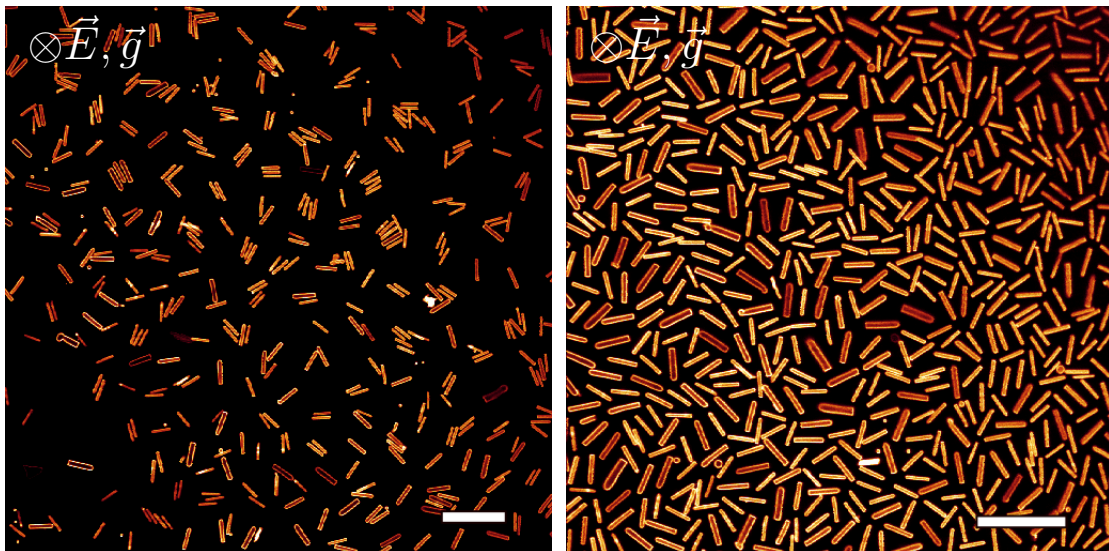
(c) Semi-concentrated suspension, with almost only rods lying down in the bottom layer. The rods on the bottom (image) form clusters, with standing rods on top of these clusters. Images on different heights of these structures are shown in Fig. 18.

(d) Concentrated suspension, with almost only rods lying down in the bottom layer. The rods on the bottom (image) are separated from each other (not touching). On top of this bottom layer, rods stand and form strings in the direction of gravity. This structure resembles the 'flats' observed by Kuijk et al. [1]. Images on different heights of this structure are shown in Fig. 19.

Fig. 17. Bottom layer of a sample with MS1-rods in an electric field of 0.82 V/μm in four different concentrations (a)-(d), resulting in different structures. The rods lie on an electrode. Images were taken in the middle of the sample, approximately one hour after preparation. Scale bars indicate 20 μm.
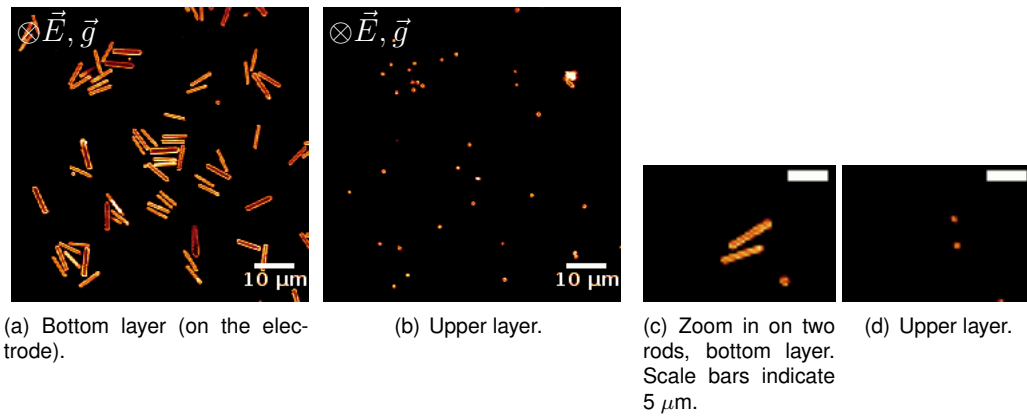
(a) Bottom layer (on the electrode).

(b) Upper layer.

(c) Zoom in on two rods, bottom layer. Scale bars indicate 5 μm.

(d) Upper layer.

Fig. 18. MS1-rods in an electric field of 0.82 V/μm of a sample with the same concentration as the sample of Fig. 26(c). The images show that the clusters in the bottom layer have aligned rods on top. Zooming in on two rods next to each other, it seems as if the standing rods in the second layer prevent pair formation. Images were taken in the middle of the sample, approximately one hour after preparation.

(a) Bottom layer (on the electrode)

(b) Second layer.

(c) Upper layer.

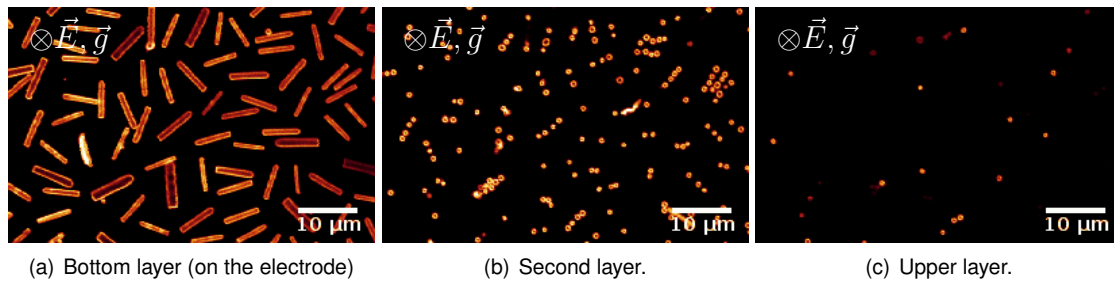**Fig. 19.** Different layers of MS1-rods in an electric field of 0.82 V/μm of a sample with the same concentration as the sample of Fig. 26(d). These images on different heights in the sample show that this concentration is sufficiently high for the rods to form flats. Images were taken in the middle of the sample, approximately one hour after preparation.

3.3   Towards a phase diagram

To increase our understanding of the necessary conditions for the observed attractions, we constructed a diagram of confocal microscope images in which volume fraction and electric field strength were varied. This was done with cells with the electrodes on the inside. This diagram, shown in Fig. 20, shows two remarkable things:

- An absence of pair formation. We did, however, reproduce the pair-structure several times. In conclusion, the necessary conditions for this structure to emerge are very delicate.

- There is an optimum in field strength for rods on the bottom of the sample to align with the field. We see that the fraction of rods lying down increases upon increasing the electric field strength.
 In our model of a rod built up of two dipoles in an electric field (section 2), the torque aligning the rod, is proportional to the electric field strength. Therefore low electric field strengths are not sufficient for a significant amount of rods to align with the field.
  On the other hand, at high electric field strengths, the potential energy of a rod ($U \sim E^2$ for a point dipole) is sufficient to overcome gravitational energy to form strings in the direction of the electric field ($\vec{E}$ and $\vec{g}$ are parallel). These strings form on top of a rod lying down. This explains the optimum in field strength for rods on the bottom of the sample to align with the field.

Phase diagram of rods in an electric field in microscope images

Down: volume fraction (in approximate ratios 1:2:5:81:162, respectively)
To the right: electric field strength (V/μm)

$\otimes \vec{E}, \vec{g}$
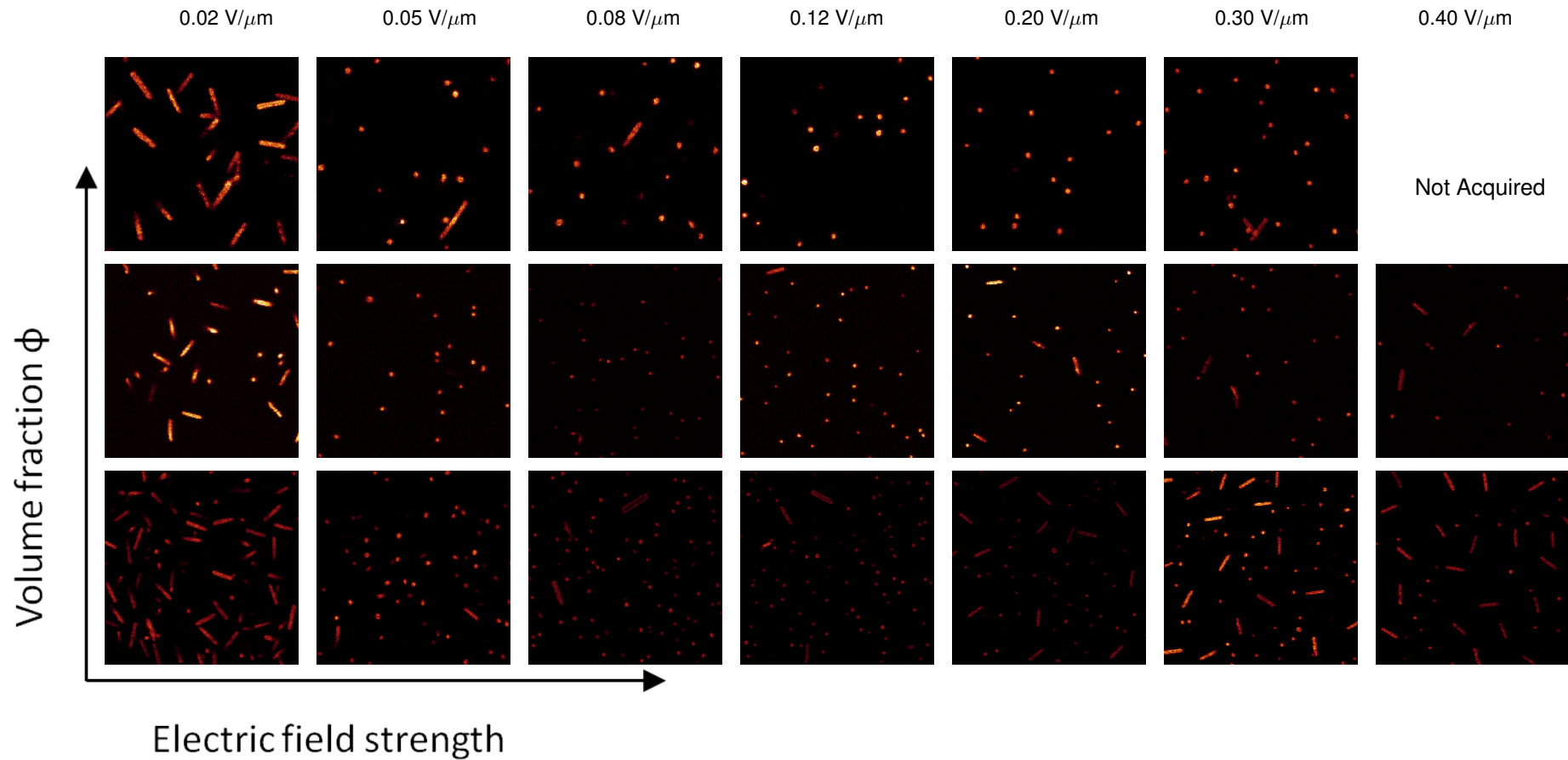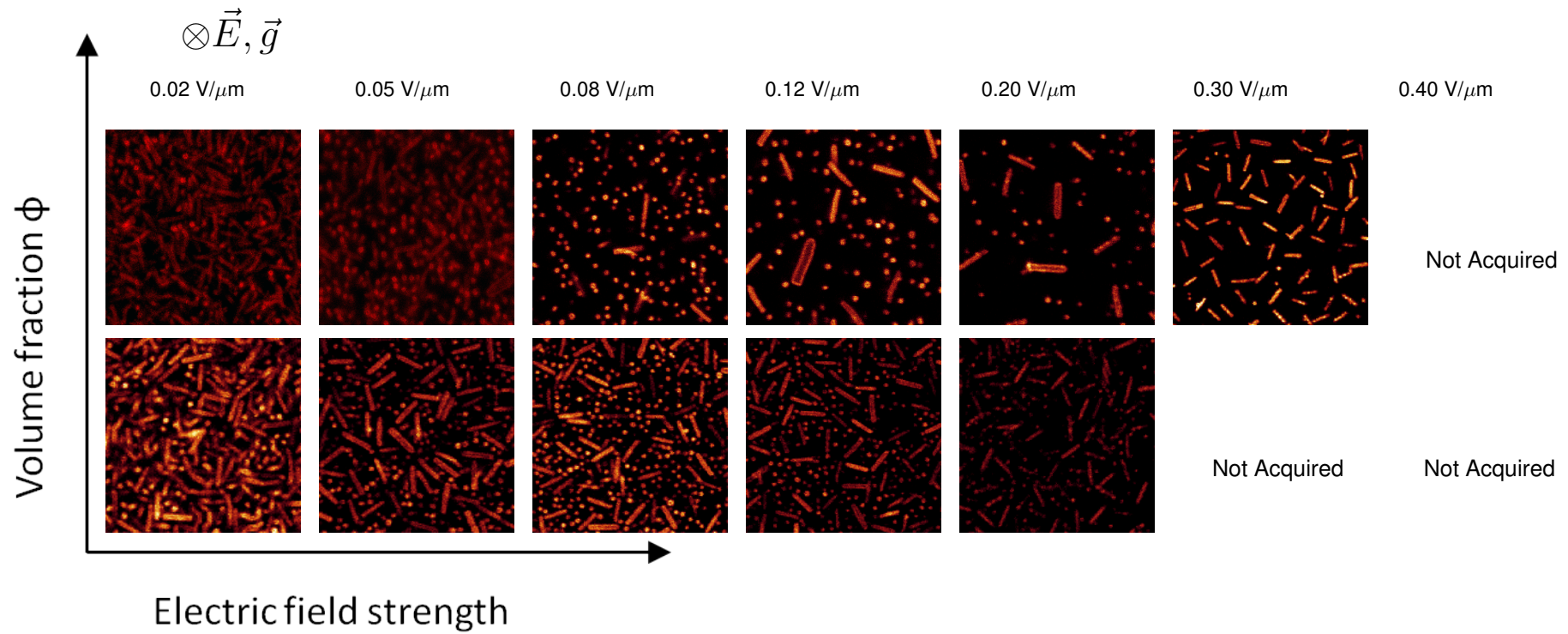
Fig. 20. The bottom layer of B35-rods in a single electric field (electrodes on the inside). Both rods lying down and rods standing up (aligning with the electric field) were observed. Moreover, flats were seen to only be formed when the concentration and electric field strength were sufficient. Note: the absence of pairs of rods in this diagram shows that the conditions necessary for pair formation are subtle. Also, we see that there is an optimum in field strength for the rods to align with the field. An explanation for this is given in the text. For some volume fractions and electric field strengths, no images were acquired because of drift in the samples due to heat development.

3.4   **The radial distribution function** $g(r)$

The radial distribution function $g(r)$ gives the probability to find a particle at a relative distance r from a given particle. It is a measure for the interactions between particles. We computed the radial distribution function for two samples of B35-rods with different concentrations in an electric field, as shown in Fig. 21. This was done by using the particle tracking software (described in section 3.1.2) which can identify the position of spheres: the aligned (standing) rods viewed from below resemble spheres (Fig. 21(a) and (c)).

We wrote a computer program in C++ (see appendix C) to compute the radial distribution function for two different concentrations:

1. In the first sample, shown in Fig. 21(a)-(c), concentration is such, that rods hardly stand on top of each other. Nonetheless, the concentration is sufficient for the particles to influence each other's motion.
   The $g(r)$ has a clear peak at $\frac{r}{D} = 1$. This indicates attractions between the rods.

2. In the second sample, shown in Fig. 21(d)-(f), the concentration in the bottom layer is higher than in the first sample. Unfortunately, we have experimentally found that this is only possible when there are rods on top of this layer as well.
   Kuijk et al. showed that these B35-rods at high concentrations in low electric fields form a C3-symmetric crystal structure (crystal where the positions of neighboring rods differ $L/3$ in height) [1]. This crystal consisted of many layers. The $g(r)$ probably shows that the pressure and concentration of the bottom layer in our sample is close to the pressure and concentration needed for such a crystal to form.
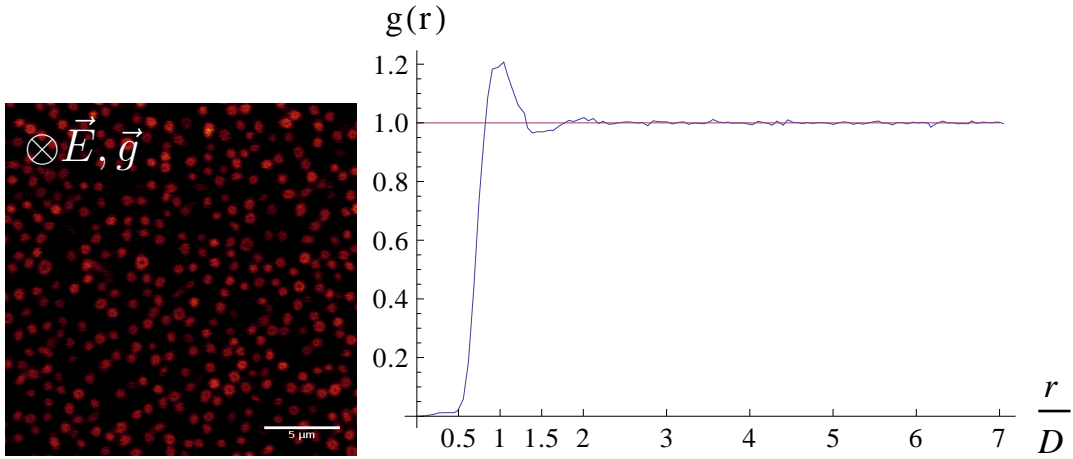
(a) The area fraction of rods is 0.19.

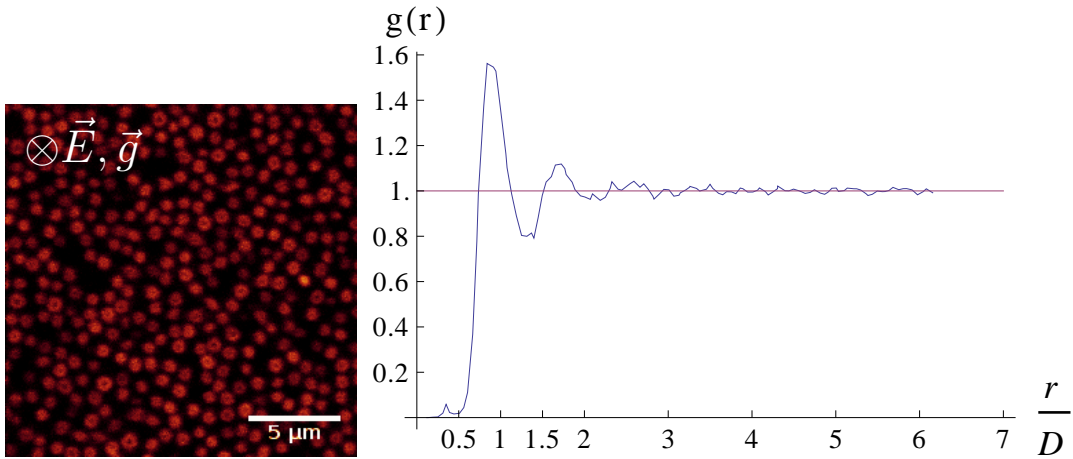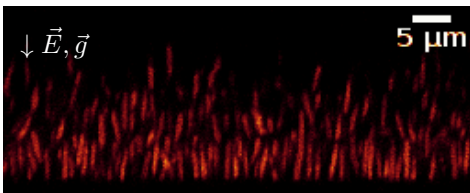(b) Radial distribution function of the bottom layer of a sample of B35-rods shown in (a) and (c), in an electric field of 0.027 V/μm. This computed $g(r)$ is the average over a thousand frames. The diameter of B35-rods is D=0.550μm.
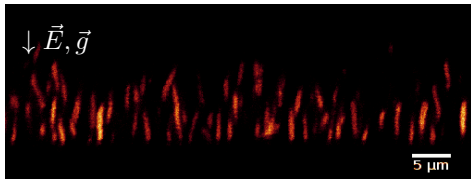
(c)

(d) The area fraction of rods is 0.24.

(e) Radial distribution function of the bottom layer of a sample of B35-rods shown in (d) and (f), in an electric field of 0.020 V/μm. This computed $g(r)$ is the average over 582 frames. The diameter of B35-rods is D=0.550 μm. The graph shows some edgy corners, so probably more samples are needed to improve statistics. The two peaks are roughly at $\frac{r}{D} = 1$ and $\frac{r}{D} = \sqrt{3} \approx 1.73$. These values are expected in a close-packed hexagonal ordering or rods. However, Fig. (d) shows that the system is not concentrated enough to be close-packed.

(f)

Fig. 21. The radial distribution functions of the bottom layer of two samples with B35-rods with different concentration. In both cases, an electric field was applied by electrodes on the outside of the cell (so the particles at the bottom are not in direct contact with the electrode). (a)-(c) In this sample, we have no really well-defined layers: the rods can be found at different heights. The $g(r)$ shows a clear peak at $r = D = 0.550\mu m$. (d)-(f) Sample with one well-defined layer with many particles on top. Its $g(r)$ shows two clearly distinguishable peaks.

4 Behaviour in a cell with two perpendicular electric fields

From experiments and theory, we know that our rods align with an applied external electric field. It is a natural attempt to first apply a horizontal electric field, resulting in rods lying flat only, and then a vertical electric field to use the formation of image charges to pull these lying rods down. The result of these actions is a two-dimensional system of rods.

The superposition of two applied external electric fields exhibits a gradient as long as it is not constant. It is known that a migration of particles is induced in an inhomogeneous electric field, as long as the dielectric constants of the solvent (ϵ_s) and the particles (ϵ_p) are unequal [16]: then a dipole moment is induced in the particle in an inhomogeneous electric field. This dipole moment leads to motion towards (if $\epsilon_p > \epsilon_s$) or away from (if $\epsilon_p < \epsilon_s$) areas with the highest electric fields. This process is called 'dielectrophoresis' [16]. In our experimental systems, we have $\epsilon_{rods} \approx 3.5 < \epsilon_s = 100$, so we expect our rods to migrate to areas with low electric fields.

However, the superposition of two constant electric fields (one in horizontal and one in vertical direction) is a constant electric field again, and dielectrophoresic forces can be excluded.

4.1 Experimental setup

A cell was constructed in which two perpendicular electric fields can be applied (see Fig. 22). This type of cell is basically an electric cell as described in section 3.1, except for two changes:

- Two wires, connected to a voltage generator, are positioned in the cell. The come into contact with the suspension.

- In order to prevent a current to flow through the electrodes resulting from contact of the wires with the electrodes, a part of the coating was etched with hydrochloric acid so that only a small strip of electrode of 3-4 mm was left.

From now on, we will call such a cell a 2-E-cell. For an elaborate guide to building such a 2-E-cell, see appendix B.
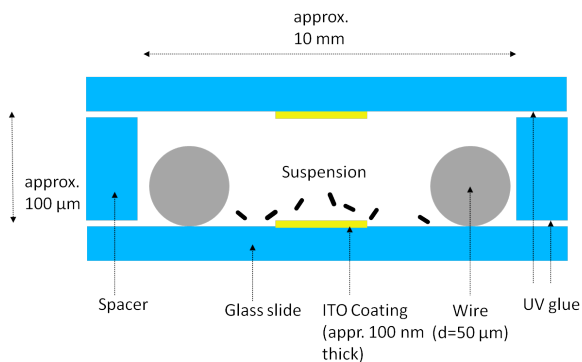
(a) Side view of a 2-E-cell.
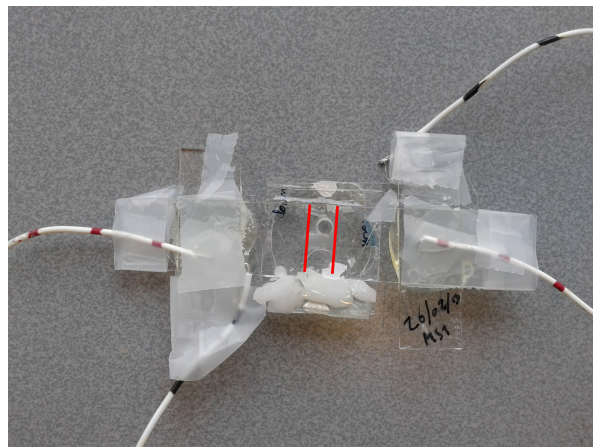
(b) Photograph of a 2-E-cell. The wires that come into contact with the dispersion are indicated in red.

Fig. 22. A cell in which two perpendicular electric fields can independently be turned on and off (a 2-E-cell). For an elaborate guide to building such a 2-E-cell, see appendix B.

4.2 Calculation of the electric field in a 2-E-cell.

A 2-E-cell consists of more than two conducting parts. Therefore, the electric potential might turn out to be very complicated. For this reason, we numerically calculate the electric field.

4.2.1 Method

The electric potential in the cell must obey the Poisson Equation,

$$\nabla^2 V = -\frac{\rho}{\epsilon_0}, \tag{23}$$

where ρ denotes the charge density. Now, we assume that there is no charge in the solvent nor in the rods. Then the Poisson Equation reduces to the Laplace equation for points in the bulk of the cell,

$$\nabla^2 V = 0. \tag{24}$$

Functions of two variables that obey the Laplace equation, so-called harmonic functions, have the property that [8]

$$V(x, y) = \frac{\oint_{circle} V \, dl}{\oint_{circle} dl} = \frac{1}{2\pi R} \oint_{circle} V \, dl \tag{25}$$

where the circle that is integrated over is the circle with radius R and center (x, y). In words, the value of the potential in a point is the average of potentials on a circle around that same point. In terms of numerical calculations, equation (25) translates to the fact that the potential in a point on a lattice is the average of the potential in the neighboring points.
The method used to calculate the electric potential is as follows:

1. We set up a lattice which models the cell.

2. We determine the boundary conditions the potential in the cell must obey and fix the potential in the corresponding lattice sites.

3. We make an educated guess for the potential in rest of the cell. (We could, for example, use the fact that the potential between two charged plates drops linearly.)

4. We apply the averaging method described above and then set the potential value in the points corresponding to the boundary conditions right again. We repeat these two steps until the solution converges.

4.2.2 Calculation

With this information, we can calculate the electric potential in the cell. We set up a 2-dimensional model of the cell (a cut through the cell), which can be seen in Fig. 23. We first take a lattice. We are looking for a solution for Laplace's equation in our cell, obeying the boundary conditions of the potential of the wires (the filled black circles in Fig. 23, which we fix at $V = +1$ for one of the wires and $V = -1$ for the other wire) and the potential of both ITO-coatings (the black lines in Fig. 23, of which the potential now follows as $V = 0$, because of the symmetry of the problem). I.e. we assume the wires and the coatings to be perfect conductors, which have the same potential everywhere. Using the method described above, we can solve this 2-dimensional problem.
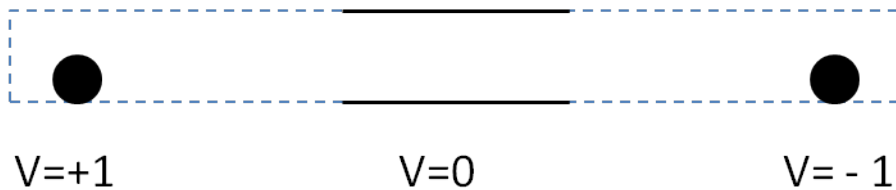
Fig. 23. 2-dimensional model for a slice of a 2-E-cell, showing the boundary conditions which the electric potential in the cell obeys.

We make an educated guess for the initial potential: we let the potential drop linearly from +1 to zero between the left side of the lattice and the beginning of the coating, then constant (at zero potential) in between the coatings, and drop linearly again – this time from zero to -1 – from the coating to the right side of the lattice.
We wrote a computer program in C to perform this calculation (see appendix C). We only look at the positions relevant to our problem, just above the lower coating (i.e. where the rods are in

our experimental samples).The electric field strength in this slice is shown in Fig. 24, and a rough schematic drawing of the field lines is pictured in Fig. 25:

1. First, we see that the field strength on the coating is practically zero. Although the wires are connected to a voltage generator, the particles located above the coating will not feel any field.

2. Moreover, there is a peak in the field strength on the border of the coating.

3. Further away from the coating, close to the wires, we have a non-zero field.[2]
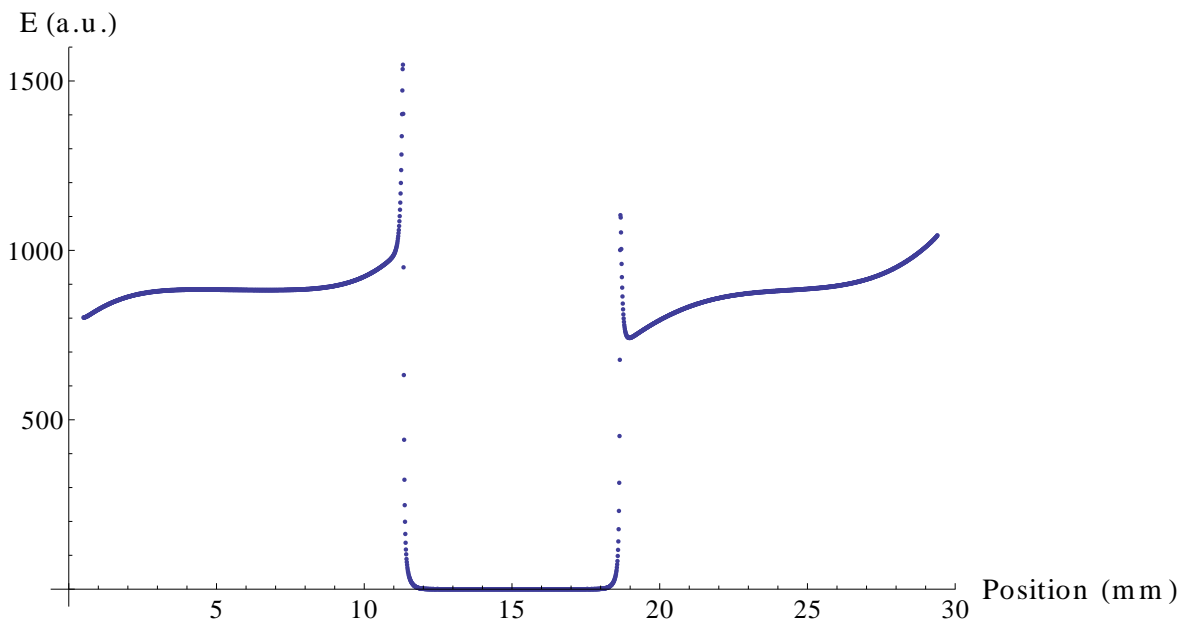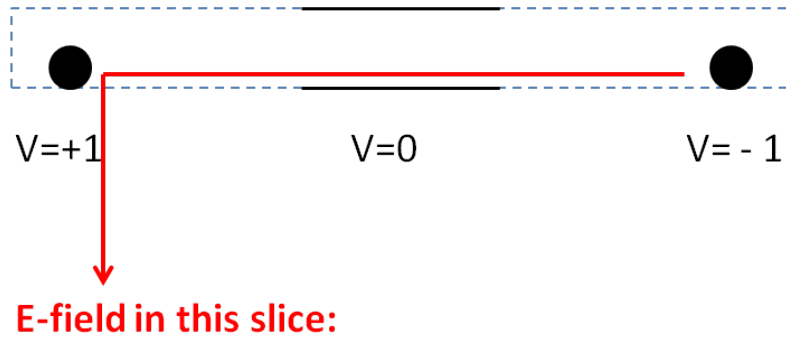
Fig. 24. Numerical calculation of the electric field strength in a slice of a 2-E-cell.

[2]Critical note: Laplace's equation does not hold entirely in our model, as there is certainly charge in the wires. However, because we are only interested in the electric field near the coating, which is far away from the wires, we can use our results far away from the wires as a fairly good approximation. The calculation consisted of 100.000 iterations, which was more than sufficient for the solution in the bulk of the lattice to converge, but this amount of iterations still was not enough for convergence near the wires.
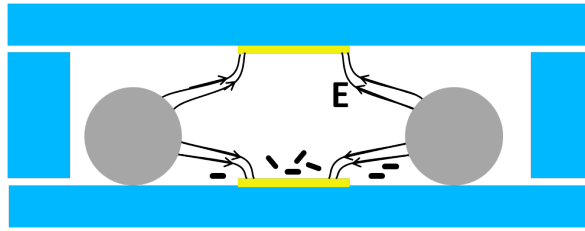
Fig. 25. Rough drawing of a few of the field lines of the calculated electric field in a 2-E-cell. The two wires are connected to a voltage generator and have opposite electric potential. The electrodes (yellow) are not connected to a voltage generator, and not to each other.

4.3   Experimental observations in a 2-E-cell.

To study the behaviour of rods in a 2-E-cell, the wires were connected to a voltage generator. The electrodes were not connected to a voltage generator, and not to each other. We distinguish between two kinds of observed structures, seen in different parts of the cell: string formation near the wires and random orientation of the rods on the electrode . These observations are shown in Fig. 26.

In some parts of the border of the electrode, we do not observe the sharp difference of alignment and isotropic behaviour as shown in Fig. 26(c), but a high concentration and smectic-like rows, as shown in Fig. 27.
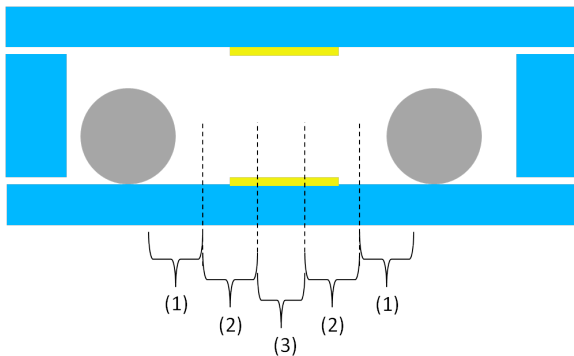
(a) Cell division in three parts.
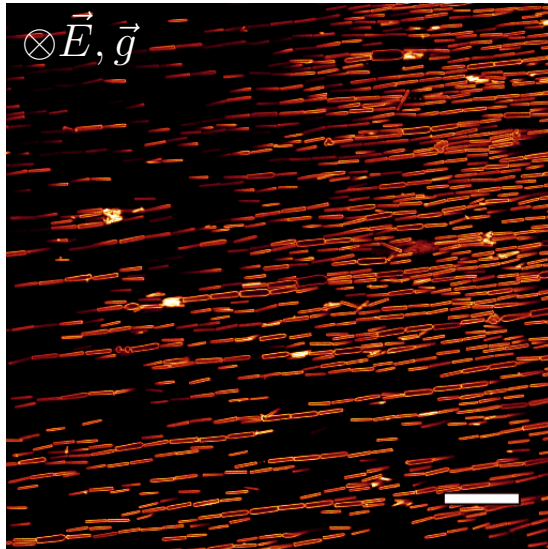
(b) **(1) Near the wires**: string formation. The wire is on the right side of this image. The gradient in the electric field strength near a wire explains why there is a concentration difference between the right and the left side of the image.
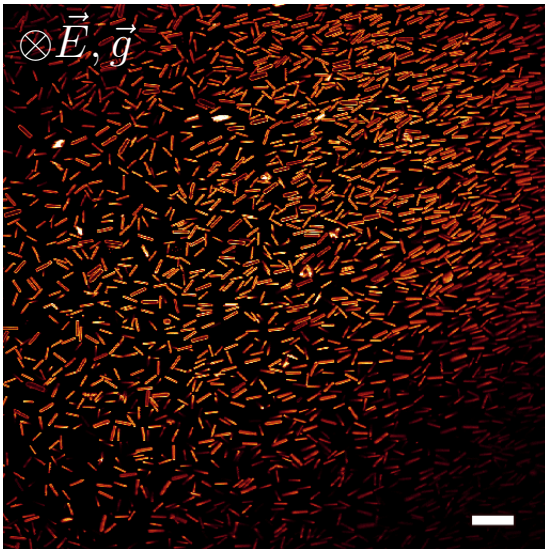
(c) **(2) On the border of the electrode**: in the right upper corner the rods feel the field of the wires (no coating), whereas in the left lower corner the behaviour is isotropic (rods are on the coated part). The hypothetical line that can be drawn in between is probably the border of the coating.
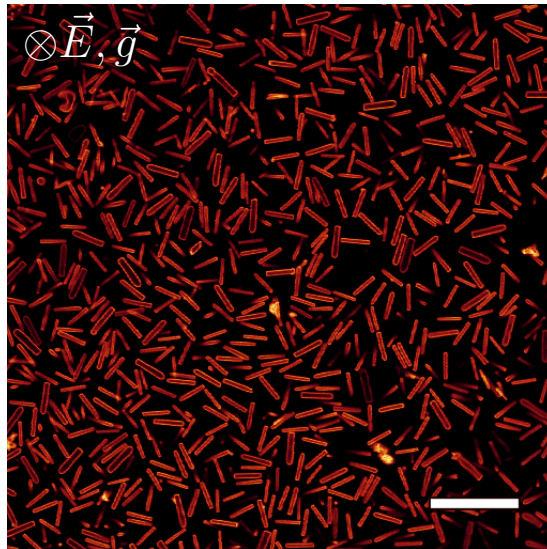
(d) **(3) On the conducting coating itself**: behaviour is isotropic. Most of these MS1-rods lie flat because they are larger than the B35-rods shown before.

Fig. 26. Different behaviour in three different parts in the 2-E-cell. Scale bars indicate 20 μm.
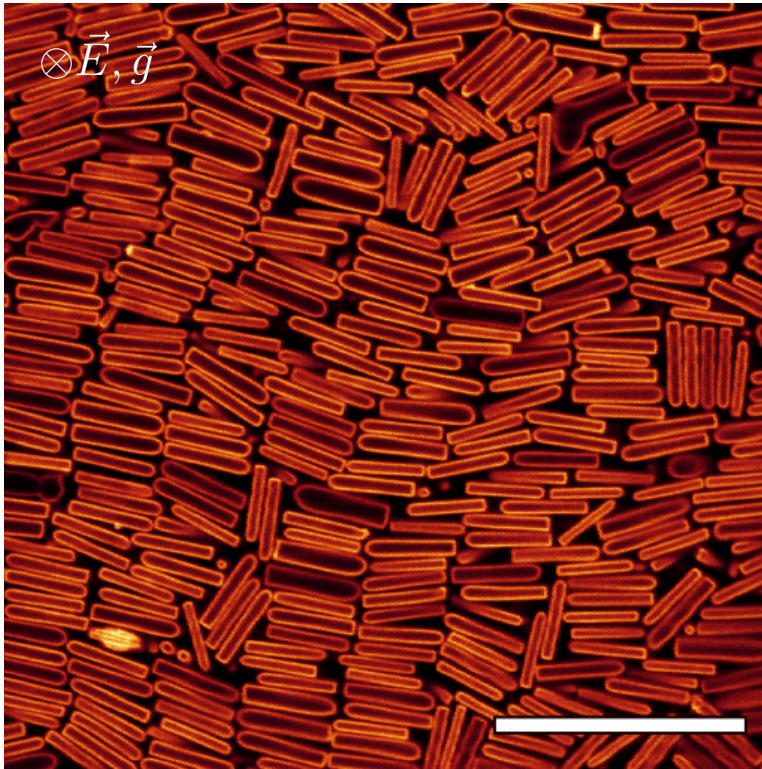
Fig. 27. At the border of the coating, at another spot than Fig. 26(c). Here, smectic-like ordering was observed. A possible explanation for the different behaviour is given in section 4.3.1. Scale bar indicates 20 μm.

4.3.1 Relation between calculations and experimental observations

We compare the experimental observations of Fig. 26 and the numerical calculations of the electric field strength (shown in the graph in Fig. 24):

- **Near the wires**
  Near the wires, it was observed that the rods align with the field and form strings. In our calculations, there was a nonzero electric field near the wires. We already expected in theory (section 2) that the electric field results in alignment and string formation of the rods.

- **On the electrodes (coated part of the glass)**
  On the electrodes, there is no electric field found in the calculation. Indeed, isotropic behaviour was observed.

- **On the border of the coated part of the glass (electrode) and the non-coated part**
 Here, two different structures formed:
  - Fig. 26(c): we can draw a sharp figurative line between an oriented part and an isotropic part in the picture. This is probably the border of the electrode.
  - Fig. 27: increased concentration. We expect this to be the result of the peak in the electric field strength found in the calculation. Removing the coating of the glass by etching with hydrochloric acid during preparation of the sample might not always result into a sharp edge of the coating: if the height of the edge drops smoothly upon getting closer to the wires, the calculated peak in electric field strength is broadened. This might explain a higher concentration of rods on the edge (see section 4.3.2).

4.3.2 Possible correlation between high (gradient of) electric field and high concentration

Behaviour on the border of the coating is not uniform: Fig. 26(c) shows different behaviour from 27. The difference between the two is probably because of the borderline of the coating not being

sharp in height.[3] The calculated electric field shows a peak at the border. A possible explanation of the formation of a smectic-like structure caused by high concentration could be the fact that the height of the ITO-coating is not uniform, resulting in a little area instead of a sharp line where the electric field strength is large (broadening of the calculated peak in Fig. 24). The attraction of the rods by the wires seen in Fig. 26(b) is another indication for a possible correlation between the gradient in the electric field and the concentration: where the electric field is high, or changes rapidly, concentration is higher too.

In conclusion, the 2-E-cell cannot be used to obtain a two-dimensional system of rods. However, the difference in electric field strength has a remarkable effect on the concentration of rods, which we can only partly explain.

---

[3]As described in the guide to building a 2-E-cell, section B, we put the coated glass in a bottle with HCl to remove part of the coating. Unfortunately, some of the HCl evaporates and damages part of the coating that is not in the solution, leaving a smooth borderline instead of a sharp edge. In line with this, we expect that the borderline in not sharp in height as well.

5 Sample preparation with electric fields for STED microscopy

In the history of microscopy, it has been a major task to increase resolution as much as possible. A recent invention has been a breakthrough in these efforts: in 1996 Hell et al. described a method of stimulated emission depletion microscopy (STED) that can break the diffraction limit [17]. This high-resolution microscopy has great potential, for example in imaging biological tissues. Samples with our rods, which have a fluorescent shell, can be a suitable calibration standard for STED microscopes.
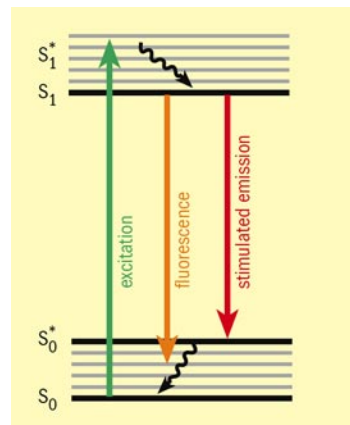
5.1 Operating principle of STED microscopy

In comparison with the single excitation laser of a usual confocal microscope, STED microscopy uses a second laser for depletion (see Fig. 28). A donut-shaped depletion laser beam with a higher wavelength than the excitation laser (in red in Fig. (a), number 7) passes through the sample roughly at the same time the excitation laser beam does. This laser light stimulates the emission of photons in fluorescent molecules at the same wavelength (in red, Fig. b), thus depleting the fluorescence. In this way, a normal fluorescent spot in the middle and a fluorescent donut-shaped ring around this spot, emitting at a higher wavelength, is obtained. As the scanner only detects the lower wavelength, resolution is increased in comparison to normal confocal microscopy [17].

Also, pulsed lasers can be used. Reflection of the incoming laser light is faster than the process of the excitation of electrons and the following emission of photons. It is useful to start detecting the light from the sample after the reflection of laser light, but before the fluorescent light from the sample arrives at the detector. This detection during a fixed interval is called time-gated STED (gSTED), as opposed to continuous-wave STED (CW-STED). For this time-gated STED, a pulsed laser is needed.
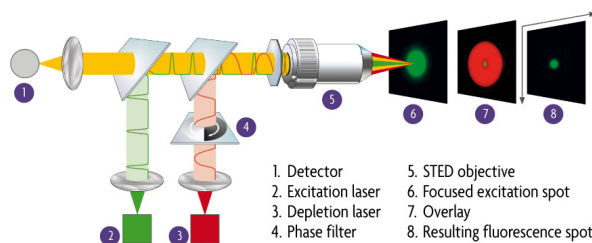
(a) Schematic view of a STED microscope. Image courtesy of Leica Microsystems.

(b) Schematic view of energy levels of electrons in dye molecules. Image courtesy of Max Planck Institute of Biophysics.

Fig. 28. The operating principle of stimulated emission depletion (STED) microscopy. Conventional microscopes use a single laser only. STED microscopy uses a second one, the so-called depletion laser. Its laser light is directed into a donut-shaped beam (in red, Fig. (a), number 7). This laser light of a higher wavelength stimulates excited electrons to excite a photon of the same wavelength while falling to a lower energy level (in red, Fig. a). This lower wavelength (red, Fig. a) differs from the wavelength that is scanned for (Fig. a, in orange). Thus the measured light originates from a smaller point (the 'hole' in the donut) only.

5.2 Deconvolution of microscope images

Scattered light within microscopes results in an optical deformation of the image of a sample (convolution of the incoming light). This response is usually described by a point spread function (PSF), a mathematical function that describes the deformation of the pathway of a theoretical point source of light. Deconvolution is the process of reversing this deformation, which can be performed using various techniques. It is capable of increasing the resolution of microscope images, removing noise and increasing contrast [18].

5.3 Useful samples for calibrating microscopes

Our rods are synthesized with a non-fluorescent inner core and outer shell and a fluorescent shell in between (see Fig. 29). Therefore, the rods are useful in test samples to obtain information of the resolution of a microscope. Fig. 30 shows different confocal microscope images of a the bottom of a sample of very concentrated sample of B35-rods, aligned with the field. Of most rods, the fluorescent shell is visible as a ring. The width of the fluorescent shell as imaged by the confocal microscope is a measure for its resolution. Imaging such systems of aligned rods also enables us to tune (calibrate) the necessary parameters of the microscope to maximalize the resolution.

From Fig. 30a it is clear that confocal microscope images of this sample without STED are distorted; of some rods, the inner core is not visible. Fig. 30c shows that using STED, resolution increases significantly: not only are the inner cores well visible, but the width of the fluorescent shells has decreased in comparison to Fig. 30a, the confocal microscope image without the use of STED. Lastly, a deconvolution of Fig. 30a, shown in Fig. 30b, decreases the distortion. The result is an image with increased resolution and contrast and less noise. Deconvolution can not contribute significantly to the resolution of our STED images; a deconvolution of the STED confocal microscope image, Fig. 30c, shows hardly an increase in resolution. On the other hand, contrast is higher and the amount of noise is reduced.
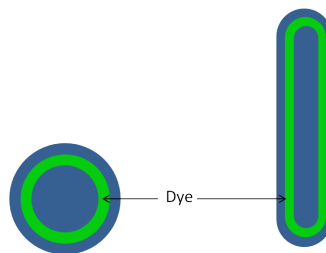
Fig. 29. Schematic view of a rod on its long and short axis. The fluorescent (FITC) layer of the B35-rods, with a thickness of 30 nm, is indicated in green.

36

(a) Confocal microscope image without STED.

(b) Image (a) after deconvolution.

(c) Confocal microscope image with stimulated emission depletion (STED). The depletion laser intensity was 100% and the laser pulses were time gated between 0.70ns and 6.14ns.

(d) Image (c) after deconvolution.

Fig. 30. Confocal microscope images of a concentrated sample of B35-rods, aligned with an electric field. Images were made with a Leica SP8 confocal microscope.

6   Discussion and conclusions

In view of our aim to obtain a two-dimensional system of rods, the distribution of the angle of B35-rods with an external electric field, perpendicular to the electrode, was measured. The distribution showed a peak for rods aligned with the field, as expected in theory. However, only a small fraction of the B35-rods lied down on the electrode. This was probably due to thermal motion of the rods in height. From the small well around the local minimum in potential energy for rods lying down on the electrode, as predicted by the calculations of Kwaadgras et al. [10], it is expected that a significantly higher fraction of rods lies down if larger rods are used, with a lower gravitational length. Our observations with the larger MS1-rods, which have a gravitational length of less than 10% of their diameter, confirmed this expectation. Moreover, the average time needed for MS1-rods to diffuse over a distance equal to their length is approximately 1.5 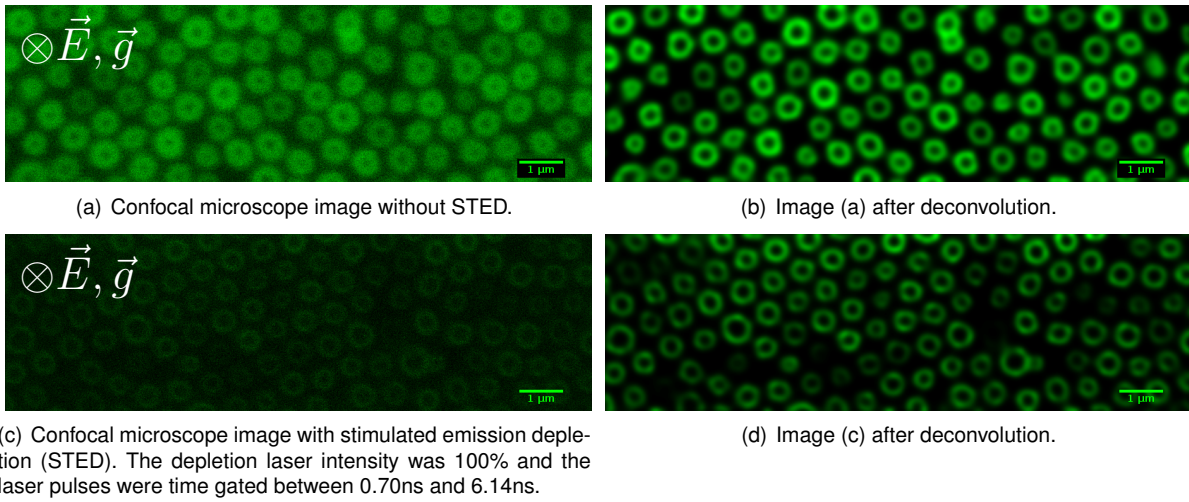minute, which is still fast enough for experiments to be realizable in time. In line with these both theoretical and experimental results, it should be possible to obtain a two-dimensional system through the use of even larger rods. In combination with the use of an electric field created by two parallel electrodes, their lower gravitational length should be sufficient to have the rods end in up the local minimum in potential energy. Thus the rods hardly move in height, thereby creating a true two-dimensional system.

Pairs, clusters, flats and more complex figures of rods in an electric field were observed. These structures disappeared by diffusion when the electric field was shut down. It was shown that pair formation does not depend on the closeness of the electrode. The observations in samples where rods are far away from an electrode are remarkable; Kwaadgras et al. have shown that there is a small attraction of rods towards a conducting plane, provided that distance between them is sufficiently small, as described in section 2.4 [10]. However, in our samples, the rods were separated from the electrode by layer of glass with a thickness of more than 100 μm. The effect of induced image charges in the electrode is then expected to be negligibly small, if any at all. The rods are therefore expected to align with the electric field instead of lying perpendicular to it. However, it was seen that a significant fraction of the rods laid down on the bottom of the sample.

Moreover, at the end of section 2 we concluded from our models that two parallel rods repel each other. The observed pair formation is in contradiction with this theory. Pair formation was tunable with the electric field; as soon as the external electric field was shut down, the rods that formed a pair started to move in a random fashion as expected in Brownian motion. Pairs of rods in the absence of an electrode seemed more 'floppy' than when the rods were on an electrode, indicating that their potential energy was of the order of their thermal energy, several $k_b T$. The fact that the former pairs seemed to be less attracted to each other, indicates that the induction of image charges in the electrode plays a positive role in the attraction that causes pair formation.
The necessary conditions for pair formation to take place are concluded to be delicate. It was shown that at least the concentration determines what structures emerge: for pairs concentration should not be too low (no interaction between the particles) nor too high (interaction is too high so that flat formation becomes energetically more favorable).

It is expected that cluster formation, which was only observed with the larger MS1-rods, is a result of the same attraction that causes pair formation. The attraction is expected to be stronger because of the larger size of the rods. However, no firm conclusions can be drawn yet. More research is to be done in elucidating the necessary conditions for pair, cluster and flat formation in terms of concentration, electric field strength and particle size.

The attraction in the bottom layer seems to be turned into a repulsion as soon as concentration is sufficient to form a second layer. This second layer always consists of standing (aligned) rods, as predicted by the results of Kwaadgras et al. (increasing distance from the electrode leads to a greater probability of alignment). It was observed that pairs hardly ever had standing rods on top. Also, flats formed smectic-like rows with a repeating interparticle spacing, indicating a repulsion. The concentration in between the concentration needed for pairs and for flats leaded to cluster formation. Our observations show a more or less repeating intercluster distance, providing evidence for a repulsive force between the clusters. It is an interesting question if these clusters perform Brownian motion as a unit on their own. This would give extra indications for the fact that lying rods attract, but lying rods with standing rods on top repel.

Parallel standing rods are expected to repel each other because of induced polarizability in the direction of the electric field. The repulsive force of standing rods could not be determined by extracting the radial distribution function from a single layer of standing B35-rods; their gravitational

38

length was too large to have a quasi-2D system of standing rods. The height difference between two neighboring rods can lead to more complicated interactions which turn from repulsive into attractive, such as in a C3-crystal. However, this indicates that the forces between aligned rods in an electric field are small. The obtained radial distribution functions might give new information on the forces when compared to computer simulations of rods with chosen force fields.

As to the formation of figures such as triangles, squares and pentagons of rods: appendix A describes the formation of emulsion droplets caused by a reaction between the solvent (DMSO) and the UV-glue used to seal the sample. These emulsion droplets form prohibited areas for rods on the bottom, causing seemingly-attracting structures of rods touching with their ends – without an electric field. However, in samples with an electric field, the disappearance of the triangles, squares and pentagons when turning off the electric field indicates an electric-field-induced attraction of rods towards such emulsion droplets. Although all samples were imaged with confocal microscopy approximately an hour after preparation, some emulsion droplets might have formed already, resulting in the observed more complex figures.

In order to obtain a two-dimensional system of (lying) rods, an electric cell with two perpendicular electric fields was used. Calculation of the electric field and experimental results showed that the electric field caused by two wires vanished in the vicinity of the electrodes. This shows that the original aim of first aligning rods parallel to the electrode and then pulling them down by the force caused by the formation of image charges cannot succeed with this particular electric cell. However, the calculation exhibited a sharp peak of the electric field strength at the border of the electrode. There are free calculation packages available which solve the differential equations for the electric potential which use roughly the same methods[4]. These better suited equation solvers can be used to confirm that there indeed is a peak in electric field strength at the border of the electrode, and that it is not a flaw in our calculation. At the same spot, an increased concentration was observed. This last fact is in disagreement with the theory, which predicts a repulsion of the particles from areas with a high electric field. This experimental observation was done only once. More research into this can confirm if the calculated potential and experimental observations. If so, we have found a way to create a step function of the electric field strength in a cell.

An electric field was used to align rods with a fluorescent shell and to create a system of standing rods starting to crystallize. It was shown that a sample with such a system can have great potential in terms of calibration of microscopes. In view of new microscopy techniques, such as stimulated emission depletion, and the emphasis on medical research in today's society, such samples might turn out to be very valuable.

In conclusion, our efforts in attempting to obtain a two-dimensional systems of rods have shown that this is probably possible with the use of an external electric field if sufficiently large rods are used. During our attempts, we observed that dilute systems of the used rods in electric fields can exhibit unexpected attractions. The phase behaviour of such dilute systems is not yet fully understood. Future research might provide the explanations for the fundamental features of these systems.

---

[4]An example of such a field solver is 'Poisson Superfish' [16].

References

[1] Kuijk, A., *Fluorescent colloidal silica rods* (PhD Thesis), Utrecht University (2012)

[2] Kuijk, A., Byelov, D.V., Petukhov, A.V., Van Blaaderen, A., Imhof, A., *Phase behavior of colloidal silica rods*, Faraday Discuss., 159, 181-199 (2012)

[3] Bates, M. A. & Frenkel, D. *Phase behaviour of two-dimensional hard rod fluids*, D. J. Chem. Phys. 112, 10034 (2000)

[4] Bolhuis, P. & Frenkel, D. *Tracing the phase boundaries of hard spherocylinders*, J. Chem. Phys. 106, 666 (1997)

[5] Rotunno et al. *Phase behavior of polarizable spherocylinders in external fields* , J. Chem. Phys. 121, 5541 (2004)

[6] Venermo, J. & Sihvola, A. *Dielectric polarizability of circular cylinder*, A. Journal of Electrostatics, 2, 63. (2005)

[7] Zheng, Z. & Han, Y., *Self-diffusion in two-dimensional hard ellipsoid suspensions* , J. Chem. Phys. 133, 124509 (2010)

[8] Griffiths, D. *Introduction to Electrodynamics*. Prentice-Hall, Inc., New Jersey, 3rd edition (1999).

[9] The calculation of two dipoles in an electric field up to equation (19) was done in private communication with Arnout Imhof, Soft Condensed Matter, Utrecht University.

[10] Kwaadgras, B., (PhD Thesis), Utrecht University (2013)

[11] Personal communication with Bas Kwaadgras, Soft Condensed Matter, Utrecht University.

[12] Kuijk, A. et al. *Synthesis of Monodisperse, Rodlike Silica Colloids with Tunable Aspect Ratio*, J. Am. Chem. Soc., 133, 2346 (2011)

[13] Computer program able to track spherical particles in confocal microscope images. The program was written by Thijs Besseling and Michiel Hermes in the Soft Condensed Matter group at Utrecht University. To be published (2013).

[14] Crocker, J.C. & Grier, D.G., *Methods of Digital Video Microscopy for Colloidal Studies* , J. Colloid Interface Sci. 179, 298 (1996)

[15] Dassanayake, U., Fraden, S. & Van Blaaderen, A., *Structure of electrorheological fluids*, J. Chem. Phys., 112, 3851 (2000)

[16] Leunissen, M., *Manipulating colloids with charges & electric fields* (PhD Thesis), Utrecht University (2007)

[17] Hell, S.W. & Wichmann, J., *Breaking the diffraction resolution limit by stimulated emission: stimulated-emission-depletion fluorescence microscopy*, Optics Letters, Vol. 19, Issue 11, 780-782 (1994)

[18] *Image Restoration*, on *www.svi.nl*. Viewed at June 15, 2013.

7   Acknowledgements

A Experimental notes: on reacting DMSO and glue

When our samples were let to rest for a day or more, strange structures were observed, shown in Fig. 31. It turned out that these were probably caused by emulsion droplets of glue, due to the reaction of the solvent (DMSO) with the UV-glue.

This reaction of DMSO with the UV-glue can be seen by a faint white glow where the solvent touches the glue (Fig. b). This reaction probably resulted in the formation of emulsion droplets on the bottom of the sample, which were visible in the confocal microscope under visual light (Fig. c). These emulsion droplets are approximately of the same size as the rods. When turning the laser light on, it was observed that the rods are positioned at the borders of the emulsion droplets only (Fig. d); the particles assemble at the foot of the 'hills' these droplets form. The resulting structure is the observed chicken-wire structure.
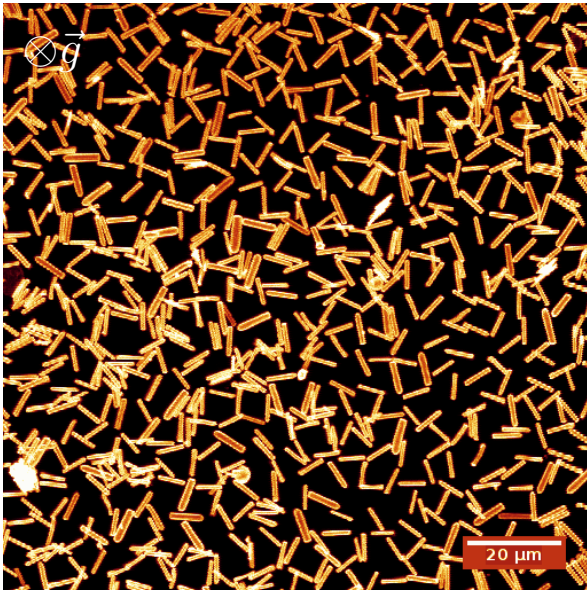
(a) Bottom layer of MS1-rods in an electric cell, put away without a field for a day.
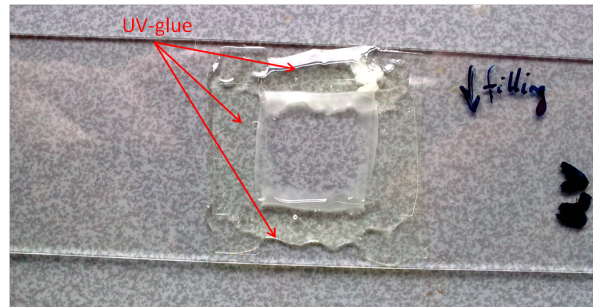
(b) Photograph of a sample filled with DMSO only. The square in the middle is filled with solvent, the surrounding square consists of glue. A faint white glow at the places where the solvent and the glue touch is clearly visible. Picture taken 1 hour after filling.
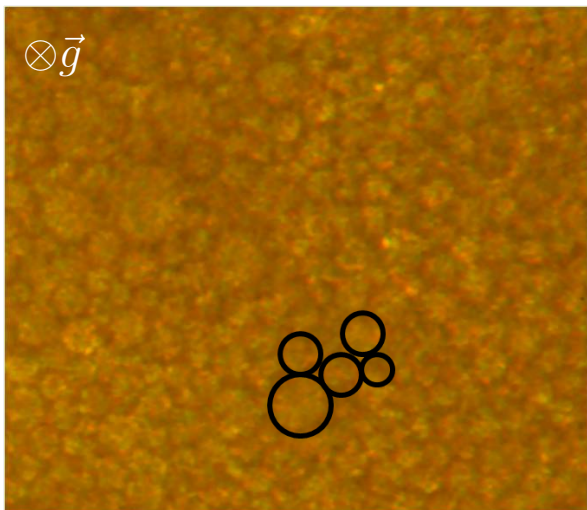
(c) Emulsion droplets on the bottom of a sample of B35-rods dispersed in a DMSO/water mixture visible under visual light in the confocal microscope.
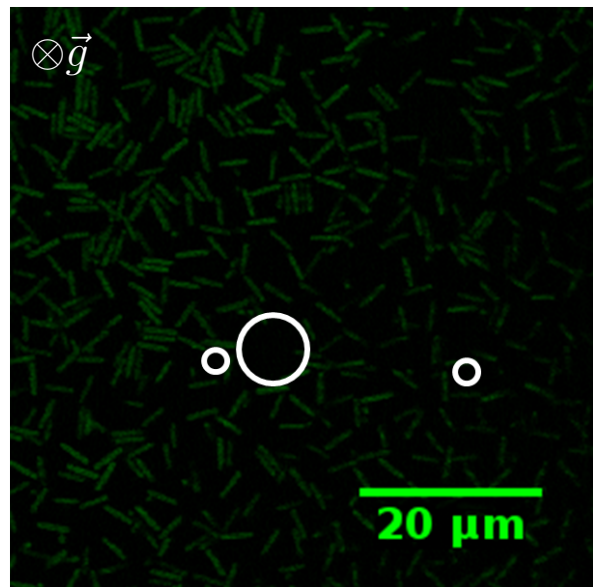
(d) Image of bottom of the same sample as in Fig. (c), using the fluorescent properties of the dyed rods in the confocal microscope. The emulsion droplets, which are only visible under visual light, are indicated as white circles.

Fig. 31. When an electric cell filled with a dispersion of rods was put away without a field for more than a day, a chicken-wire like structure was observed (Fig. (a)). This was probably caused by the reacting solvent (DMSO) with the UV-glue; a faint white glow can be seen where the solvent comes into contact with the glue (Fig. (b)). This reaction probably resulted in the formation of emulsion droplets on the bottom of the sample, which were visible in the confocal microscope under visual light (Fig. (c)). Sedimenting rods fall down to the foot of the 'hills' these droplets on the bottom are. The size of these droplets is of the same order of magnitude as the length of the rods, resulting in the observed chicken-wire structure (Fig. (d)).

B   Building a cell with two electric fields

B.1   Preparing glass slides with a conducting strip

In building a cell with two electric fields (a 2-E-cell), glass slides with one side coated with a conducting material (usually ITO) were used. First the conducting coating was etched with hydrochloric acid ($3.0 \; mol \cdot L^{-1}$). This was done by letting the glass slides stand vertically in a glass filled with the hydrochloric acid solution. It took approximately 1.5 minute for the acid to remove the coating. Leaving it for a longer time causes the acid to evaporate, which could damage the coating at the part where it is not touched by the acid. By repeating this procedure with the coated glass slide turned around, a glass slide with a coated strip only was obtained. The coated strip was approximately 4 mm in width.

B.2   Building the cell

See figure 32.

(a) An etched glass slide, prepared as described above, with the coated side pointing upwards was used. Which side is coated, can be checked with a resistance meter; the side that gives a nonzero value for resistance, is the coated side. Next, two small rectangular pieces of glass spacers were glued next to the coated strip (Fig. 32(a)). Two wires were placed in between the strip and the rectangular pieces (as indicated in the figure). The glass slides were not glued yet, but the wires were laid loosely on top of the glass slide.

(b) Next, another etched glass slide was glued on top of this, with its coated side pointing downwards (towards the rest of the cell). This one was positioned slightly out of place, such that it sticked out on one side (Fig. (a)).
It is important that the wires do not touch the coating. Also, the distance between the wires was taken not much more than a centimeter for the electric field to be strong enough.

(c) Each of the loose wires were connected with itself as indicated in Fig. 32(b). After this, another wire was wound around the bottom glass slide as in Fig. 32(c). This procedure was repeated for the upper glass slide. As a result, one had four different loose wires. They did not touch.

(d) After this, a glass slide was cut into two parts in length. The entire cell prepared as described above was glued on the middle of a part of the glass slide. To reduce the probability of breaking the parts sticking out, half a glass slide was glued to the left and to the right of the glass slides (Fig. 32(d)). Lastly, all four wires were put into place as indicated in the figure, and kept in place with duct tape.
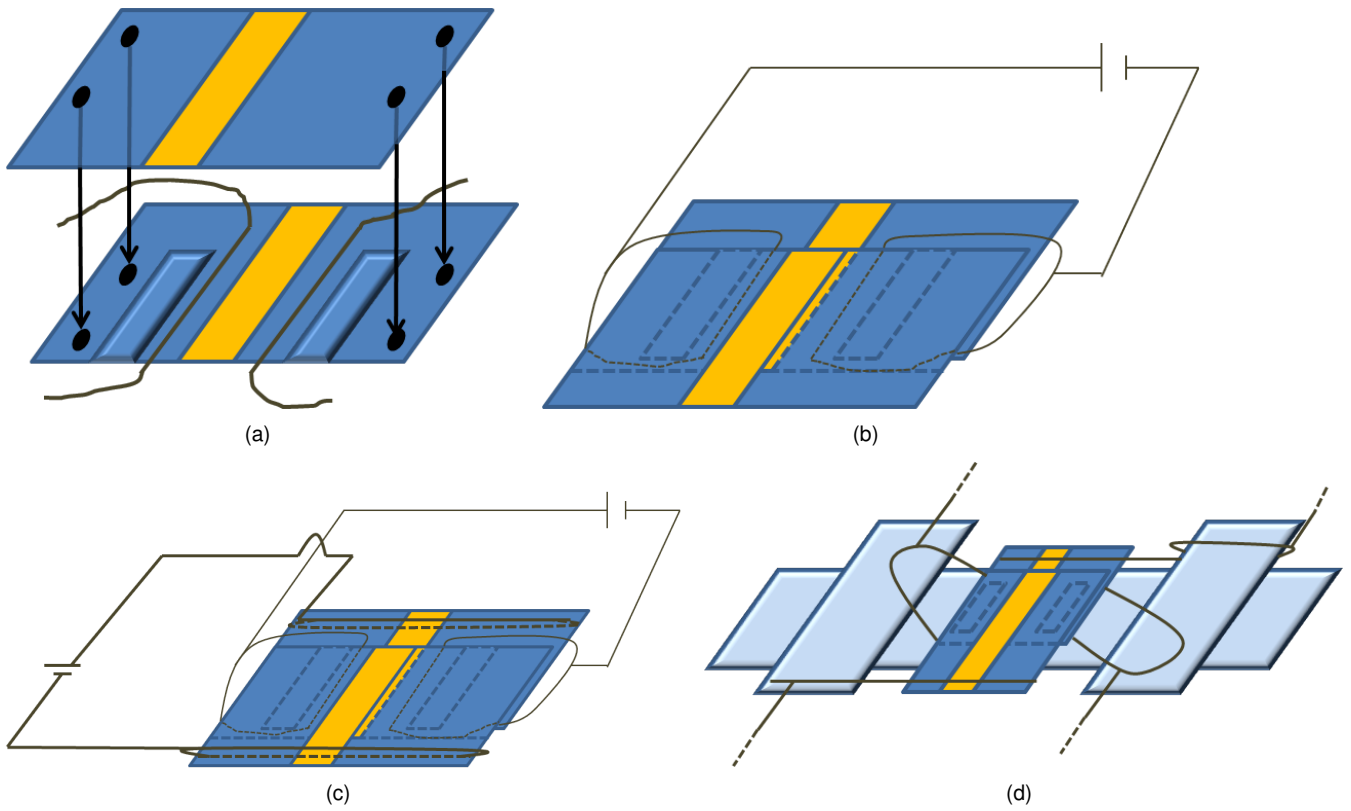
(a)

(b)

(c)

(d)

Fig. 32. Building a 2-E-cell. The building steps are explained in the text.

C   Computer codes for calculating the radial distribution function and the electric potential

C.1   C++ code for calculating the radial distribution function

```cpp
#include <sstream>
#include <string>
#include <iostream>
#include <fstream>
#include <stdio.h>
#include <stdlib.h>
#include <sys/types.h>
#include <sys/stat.h>
#include <unistd.h>
#include <math.h>

#define DELTAR 2
#define RMIN 0.0001 //may not be zero
#define RMAX 200.0
#define BOXSIZE 256

using namespace std;

int main(){

//get filename of picture, which is stored in the file "inputgr.in"
string filenaam, filenaam2;
ifstream f("./inputgr.in");
while( f.good() )
        {
        getline(f,filenaam2);
        filenaam.append (filenaam2);
        }
f.close();


//get number of particles tracked by computer program feature
ifstream file;
file.open(filenaam.c_str());
string value, naam, str, aantaldeeltjesstring;
getline (file, aantaldeeltjesstring, '\n');
int length=atoi(aantaldeeltjesstring.c_str());

//get rid of the boxsize values (we give these ourselves, see #define BOXSIZE
    getline ( file, value, '\n');
    getline ( file, value, '\n');



//get position coordinates
long double lijst[length][2];
string sx,sy;
int positerator=0;

while ( file.good() )
{
    getline ( file, value, '\n');

if(file.good()){} else{break;}

sx=string(value,0,13);
lijst[positerator][0]=atof(sx.c_str());

sy=string(value,13,20);
lijst[positerator][1]=atof(sy.c_str());

positerator++;
}

// calculate g(r)
```

45

```
int grlength=BOXSIZE/DELTAR+1,i,j,bin;
double gr[grlength];
long double drij[2],rij,Pi=4*atan(1),waarde;

for(i=0;i<grlength;i++){gr[i]=0;}

for(i=0;i<length-1;i++)
{
        for(j=i+1;j<length;j++)
                {
                drij[0]=lijst[j][0]-lijst[i][0];
                drij[1]=lijst[j][1]-lijst[i][1];
                if(drij[0]<-0.5*BOXSIZE){drij[0]=drij[0]+BOXSIZE;}
                if(drij[1]<-0.5*BOXSIZE){drij[1]=drij[1]+BOXSIZE;}
                if(drij[0]>0.5*BOXSIZE){drij[0]=drij[0]-BOXSIZE;}
                if(drij[1]>0.5*BOXSIZE){drij[1]=drij[1]-BOXSIZE;}

                rij=drij[0]*drij[0]+drij[1]*drij[1];rij=sqrt(rij);
                bin=rij/DELTAR;
                gr[bin]=gr[bin]+2;

                }
}

double rlower,rupper,nideal;
for(bin=0;bin<grlength;bin++)    {
                                 rlower=bin*DELTAR;
                                 rupper=rlower+DELTAR;
                                 waarde=rupper*rupper-rlower*rlower;
                                 nideal=Pi*waarde*length*length/(BOXSIZE*BOXSIZE);
                                 gr[bin]=gr[bin]/nideal;
                                 }


//output
cout<<length<<endl;
for(int lijstiterator=0;lijstiterator<RMAX/DELTAR;lijstiterator++)
{
        cout<<gr[lijstiterator]<<endl;
}

return 0;
}
```

C.2   C code for calculating the electric potential in a 2-E-cell

```c
#include <stdlib.h>
#include <stdio.h>

#define RIJ 45
#define KOLOM 3000
#define D 1125 //distance between center of the wire and coating border
#define radius 8


int main(int argc,char *argv[])
{
double N=atof(argv[1]);

double V[RIJ][KOLOM],klad[RIJ][KOLOM],difference[RIJ][KOLOM];
double f,diff,lastdiff=10,a1,a2,b1,b2;
int i,j,k=0;

//initial values
for(i=0;i<RIJ+1;i++){for(j=0;j<KOLOM+1;j++){V[i][j]=0;}}

f=D+radius;f=1/f;

for(i=0;i<RIJ+1;i++){for(j=0;j<D+radius+1;j++){
        V[i][j]=-f*j+1;
        V[i][j+1+KOLOM-D-radius-1]=-f*j;
}}
//klad=V
for(j=0;j<KOLOM;j++)
{
        for(i=0;i<RIJ;i++){klad[i][j]=V[i][j];}
}

//<-------start of averaging procedure
for(diff=3.3;k<N;k++)
{
        diff=0.0;

//Averaging points in the bulk
        for(j=1;j<KOLOM-1;j++){for(i=1;i<RIJ-1;i++){
                klad[i][j]=(V[i][j-1]+V[i][j+1]+V[i-1][j]+V[i+1][j])/4;
                lastdiff=klad[i][j]-V[i][j];
                if(k==N-1&&lastdiff!=0){printf("%f\n",lastdiff);}
                if(diff<lastdiff){diff=lastdiff;}
                //printf("%lf %lf %lf %lf\n",klad[i][j],V[i][j],diff,lastdiff);
        }}

//Averaging borders, but without the corners
        i=0;
        for(j=1;j<KOLOM-1;j++)
        {
                                        klad[i][j]=V[i][j-1]+V[i][j+1]+V[i+1][j]; //zonder V[i-1][j]
                                        klad[i][j]=klad[i][j]/3;
                                        lastdiff=klad[i][j]-V[i][j];
                                        if(k==N-1&&lastdiff!=0){printf("%f\n",lastdiff);}
                                        if(diff<lastdiff){diff=lastdiff;}
        }


        i=RIJ-1;
        for(j=1;j<KOLOM-1;j++)
        {
                                        klad[i][j]=V[i][j-1]+V[i-1][j]+V[i+1][j]; //zonder V[i][j+1]
                                        klad[i][j]=klad[i][j]/3;
                                        lastdiff=klad[i][j]-V[i][j];
                                        if(k==N-1&&lastdiff!=0){printf("%f\n",lastdiff);}
                                        if(diff<lastdiff){diff=lastdiff;}

        }
```

```
// Averaging the corners
        klad[0][0]=V[0][0+1]+V[0+1][0];klad[0][0]=klad[0][0]/2;
        klad[0][KOLOM−1]=V[0][KOLOM−1−1]+V[0+1][KOLOM−1];klad[0][KOLOM−1]=klad[0][KOLOM−1]/2;
        klad[RIJ−1][0]=V[RIJ−1][0+1]+V[RIJ−1−1][0];klad[RIJ−1][0]=klad[RIJ−1][0]/2;
        klad[RIJ−1][KOLOM−1]=V[RIJ−1][KOLOM−1−1]+V[RIJ−1−1][KOLOM−1];
        klad[RIJ−1][KOLOM−1]=klad[RIJ−1][KOLOM−1]/2;

        lastdiff=klad[i][j]−V[i][j];
        if(k==N−1&&lastdiff!=0){printf("%f\n",lastdiff);}
        if(diff<lastdiff){diff=lastdiff;}

//V=klad
for(j=0;j<KOLOM;j++)
{
        for(i=0;i<RIJ;i++){V[i][j]=klad[i][j];}
}

// wires
for(j=0;j<KOLOM;j++){for(i=0;i<RIJ;i++)
{
        a1=(i−radius+1);b1=(j−radius+1);
        a2=(i−radius+1);b2=(j+radius−1−KOLOM+1);
        if(a1*a1+b1*b1<radius*radius){V[i][j]=1;}
        if(a2*a2+b2*b2<radius*radius){V[i][j]=−1;}
}}

//ITO−coating
        for(j=radius−1+D;j<KOLOM−radius−1−D;j++){V[0][j]=0;}
        for(j=radius−1+D;j<KOLOM−radius−1−D;j++){V[RIJ−1][j]=0;}


} //<−−−−end of averaging procedure

// output
for(j=0;j<KOLOM;j++)
{
                for(i=0;i<RIJ;i++){        printf("%f",V[i][j]);
                                        if(i!=RIJ−1){printf(",␣");}
                        }
if(j!=KOLOM){printf("\n");}
}


return 0;
}
```

48